Clim Dyn
DOI 10.1007/s00382-017-3946-9

Australian snowpack in the NARCliM ensemble: evaluation, bias correction and future projections

Alejandro Di Luca[1] · **Jason P. Evans**[1] · **Fei Ji**[2]

Received: 27 February 2017 / Accepted: 2 October 2017

Abstract In this study we evaluate the ability of an ensemble of high-resolution Regional Climate Model simulations to represent snow cover characteristics over the Australian Alps and go on to asses future projections of snowpack characteristics. Our results show that the ensemble presents a cold temperature bias and overestimates total precipitation leading to a general overestimation of the snow cover as compared with MODIS satellite data. We then produce a new set of snowpack characteristics by running a temperature based snow melt/accumulation model forced by bias corrected temperature and precipitation fields. While some positive snow cover biases remain, the bias corrected (BC) dataset show large improvements regarding the simulation of total amounts, seasonality and spatial distribution of the snow cover compared with MODIS products. Both the raw and BC datasets are then used to assess future changes in the snowpack characteristics. Both datasets show robust increases in near-surface temperatures and decreases in snowfall that lead to a substantial reduction of the snowpack over the Australian Alps. The snowpack decreases by about 15 and 60% by 2030 and 2070 respectively. While the BC data introduce large differences in the simulation of the present climate snowpack, in relative terms future changes appear to be similar to those obtained using the raw data. Future temperature projections show a clear dependence with elevation through the snow-albedo feedback effect that affects snowpack projections. Uncertainties in future projections of the snowpack are large in both datasets and are mainly dominated by the choice of the lateral boundary conditions.

Keywords Snowfall · Snow cover · Climate change · Mountains · High resolution

1 Introduction

The Australian alpine region is a unique climate zone as it is the only region in mainland Australia that supports seasonal snow fields. The Australian Alps are located in southeastern Australia and they include parts of eastern Victoria, southeastern New South Wales, and the Australian Capital Territory. It is the highest mountain range in Australia with elevations exceeding 2000 m.

The Australian Alps contain seasonal snow fields that are important across a number of sectors. From an economic perspective, this region is at the heart of the "Snowy Mountains Scheme". This scheme produces hydroelectric energy through sixteen major dams and nine power stations. It also collects and diverts water from snow melt inland into the Murray and Murrumbidgee Rivers for irrigation. As such, it has a significant role in securing the availability of water within the Murray–Darling Basin, one of the most important agricultural regions in Australia. Besides their importance in energy production and irrigation, the Snowy Mountains are home to a number of well developed ski resorts and snow-related tourism during the winter season.

Electronic supplementary material The online version of this article (doi:10.1007/s00382-017-3946-9) contains supplementary material, which is available to authorized users.

✉ Alejandro Di Luca
a.diluca@unsw.edu.au

[1] Climate Change Research Centre and ARC Centre of Excellence for Climate System Science, University of New South Wales, Sydney, NSW, Australia

[2] Office of Environment and Heritage, Department of Planning and Environment, Queanbeyan, NSW, Australia

Published online: 19 October 2017

From an ecological perspective, the region contains unique Australian ecosystems. The vulnerability to climate change of Australia's alpine fauna is considered to be high (Hughes 2003). Animals such as the mountain pygmy-possum may see a complete disappearance of their bioclimatic range with a temperature rise of only 1 °C accompanied by a 5% reduction in winter precipitation (Brereton et al. 1995). A number of unique alpine vegetation communities are also likely to experience distribution changes (Pickering and Armstrong 2003).

Due to their latitudinal location and relatively low elevations, the Australian Alps snow fields are particularly vulnerable to changes in the climate. Winter mean air temperatures over the Australian Alps fall within the − 5 to 5 °C range that was identified by Brown and Mote (2009) to characterise zones with the largest sensitivity to global warming. As argued by Thompson (2016), "the [Australian Alps] are likely to be amongst the first alpine areas in the Southern Hemisphere where the effects of climatic change will be observed". Indeed, a number of studies have shown that some of these changes are already being observed. Table 1 shows reported observed trends for several snowpack characteristics over the Australian Alps. Results were derived from a number of sites in the Australian Alps (Nicholls 2005; Hennessy et al. 2008; Davis 2013; Fiddes et al. 2015) and using satellite remote sensing measurements (Bormann et al. 2012a; Thompson 2016). While most of these trends appear to be statistically insignificant, they all show a consistent decrease in snowpack characteristics (e.g., snow depth and snow cover extent) suggesting that changes might be physically significant and it is just a matter of time for the trends to be statistically significant.

A number of studies investigated the impact of future climate changes on snowfall and snowpack over the Australian Alps (Whetton et al. 1996; Hennessy et al. 2008; Fiddes et al. 2015; Timbal et al. 2016). All of these studies project large decreases in snowfall and snowpack into the future (consistent with current trends) with the snow season becoming shorter and encompassing smaller areas. These decreases are largely driven by future temperature increases (Whetton et al. 1996; Timbal et al. 2016) due to the combined effect of less precipitation falling as snow and higher rates of melting/sublimation. While snowfall and snowpack projections show clear decreasing trends, regional uncertainties are still very large mainly due to uncertainties in future temperature changes related with the choice of future emission scenarios and the specific Global climate model (GCM).

An important limitation of most of these studies is that snowpack projections were produced using future climate changes from GCMs despite GCMs having virtually no representation of the Australian alpine region. A large number of studies have shown the advantages of increasing the horizontal resolution of climate models in order to improve

Table 1 Observed trends of various characteristics of the snowpack over the Australian Alps as reported in different studies

Study	Period	Observation	Snowpack characteristic	Trend (per decade)
Nicholls (2005)	1962–2002	In situ (1)	Max. SD	Decreasing (weak)
			Spring SD	Decreasing (strong)
Hennessy et al. (2008)	1957–2002	In situ (4)	Max. SD	Decreasing (weak)
			Spring SD	Decreasing (moderate)
Davis (2013)	1957–2010	In situ (1)	Max. SD	Decreasing (weak)
Fiddes et al. (2015)	1988–2013	In situ (3)	Max. SD	Decreasing (15%)
			Snowfall	Decreasing (9%)
Bormann et al. (2012b)	2000–2010	Satellite	Mean SC extent	Decreasing (35%)
		MOD-MADI	Max. SC extent	Decreasing (50%)
			Mean SC duration	Decreasing (14 days)
			Mean SC onset	Increasing (2 days)
			Mean SC melt	Decreasing (12 days)
Thompson (2016)	2000–2014	Satellite	Mean SC area	Decreasing (13%)
		MODIS-Th	Max. SC area	Decreasing (10%)
			Mean SC duration	Decreasing (10 days)
			Mean SC onset	Increasing (3 days)
			Mean SC melt	Decreasing (7 days)

For in situ observations, the number of stations is denoted in parenthesis. Trend calculations for both MODIS products were performed by the authors using the areal mean over the common MODIS-Th region. When given in percentage, trends denote the change in a decade normalized by the average over the period as specified in the second column. SC denotes snow cover and SD snow depth. As later described in Sect. 2, MOD-MADI and MODIS-Th datasets were developed by Bormann et al. (2012b) and Thompson (2016) respectively

the simulation of the climate in areas characterised by complex topography (e.g., Prömmel and Geyer 2010; Feser et al. 2011; Di Luca et al. 2013; Prein et al. 2015; Giorgi et al. 2016). Recently, Di Luca et al. (2016) assessed the value added by an ensemble of regional climate model (RCM) simulations (10 and 50-km resolutions) compared with their global driving data (about 250-km resolution) over southeast Australia. They showed that RCMs generally outperform the driving data, particularly over areas with complex terrain and for temperature variables. As such, given the strong dependence of the snowpack with temperature and precipitation fields through elevation changes (e.g., Giorgi et al. 1997; Kotlarski et al. 2012; Steger et al. 2013; Frei et al. 2017), substantial benefits are expected from an increase in horizontal resolution.

The use of high-resolution simulations is not only important to well simulate the snowpack climatology but also their plausible future changes. The future of the snowpack critically depend on future temperature changes that are strongly influenced by the snow-albedo feedback (SAF), an effect that enhances the warming through changes in the albedo of the snow-affected regions (Sellers 1969; Robock 1983; Qu and Hall 2007). The only way to explicitly represent the SAF effect is through the use atmosphere-land surface coupled models that have high enough horizontal resolution to well represent the snowpack of the region of interest.

A number of studies have assessed snowpack future changes using one-way nested, limited-area RCMs (Giorgi et al. 1997; Kotlarski et al. 2012; Steger et al. 2013; Frei et al. 2017). Steger et al. (2013) evaluated the ability of an ensemble of 18 RCM simulations to represent the snowpack over the European Alps and assessed future projections over the 21st century. They found future changes in the snowpack to depend strongly on the elevation with larger reductions over lower elevations attaining values of − 70% by the end of the century. They also found a general shortening of the snow-season duration related to both a later start but mainly an earlier melt of the snowpack. In a recent article, Frei et al. (2017) evaluated the representation of the snowfall over the European Alps using an ensemble of 14 RCM simulations. They showed that simulations were able to well simulate seasonal and spatial variations of the snowfall although they also showed significant positive biases especially at high elevations. To remove theses biases, they corrected simulated snowfall by independently correcting temperature and precipitation fields. The comparison of the climate change signal obtained from the raw and bias corrected snowfall revealed no substantial differences for the multimodel mean relative changes at different elevations.

The aims of this paper are threefold: first, to evaluate the skill of an ensemble of high-resolution regional climate model (RCM) simulations to represent the seasonally varying snow cover and other related fields such as total precipitation and temperature. Second, to assess future changes in the snowpack as simulated by the ensemble. Third, to quantify the impact of using bias-corrected temperature and precipitation fields to force a snow melt/accumulation model that simulates snow depths for present and future periods. The analysis uses data from the New South Wales (NSW) and Australian Capital Territory (ACT) Regional Climate Modelling (NARCliM) RCM ensemble (Evans et al. 2014) which is the largest climate model ensemble performed at high resolution (10 km grid spacing) over southeast Australia.

The paper is organised as follows. The next section describes the observations and the NARCliM RCM simulations. Section 3 introduces the region of analysis and seasonal descriptors use to characterise the snowpack while Sect. 4 includes a description of the various steps needed to produce a bias corrected version of the original NARCliM ensemble. Section 5 briefly discuss the observed climatology and recent trends of snowpack characteristics and related variables using satellite and gridded observations. Section 6 evaluates the NARCliM modelled results for the present period while Sect. 7 presents future projections of the snowpack and related variables. Section 8 quantifies and discusses the sources of uncertainties in the future snowpack projections. Lastly, concluding remarks are given in Sect. 9.

2 Data

2.1 Temperature and precipitation observed gridded data

Daily gridded data from the Australian Water Availability Project (AWAP; Jones et al. 2009) are used in this study as the reference dataset for precipitation and temperature variables. AWAP is a product developed by the Australian Bureau of Meteorology (BOM) consisting of daily gridded datasets of in situ measurements of minimum and maximum 2-m temperatures and precipitation. It was constructed using an anomaly-based approach to interpolate information from meteorological stations onto a 0.05° regular grid where the number of stations varies through time although with relatively good coverage in the recent period. While the AWAP dataset has been shown to be consistent with a number of high-quality station observations across Australia (King et al. 2013), some systematic errors have been identified over the Australian Alps. Chubb et al. (2015) found that the AWAP product likely underestimates total precipitation by up to 50% over the western slopes of the Australian Alps. These discrepancies are due to both a low density of BOM stations over the alpine region (and a heterogeneous spatial distribution) and to difficulties of measuring frozen

precipitation using the standard BOM precipitation gauge types, leading to significant undercatch.

2.2 MODIS snow-cover satellite data

This study characterises recent past snow-cover using two satellite products. While both products are derived using the Moderate resolution Imaging Spectroradiometer (MODIS) data, they use different algorithms to detect snow and to discriminate between snow and clouds leading to significant differences in the spatio/temporal variability of snow cover.

2.2.1 MOD-MADI dataset

The first product is here denoted as the MOD-MADI seasonal snow cover dataset and it was developed by Bormann et al. (2012a). This product uses the MODIS level-1B calibrated and geolocated radiances and a custom snow detection algorithm optimised for the Australian snow conditions. The snow detection algorithm is based on the Melt Area Detection Index (MADI) of Chylek et al. (2007) and is calculated as the ratio of reflectance values from two spectral bands in the near-infrared. MADI was originally developed to discriminate between dry and wet snow in Greenland but its application for snow detection was considered suitable due to the particular properties of snow in the Australian Alps (Bormann et al. 2012a). As reported by Bormann et al. (2012a), the implementation of MADI for snow detection purposes required extensive modifications of the thresholds used compared with values over Greenland.

In order to reduce the impact of errors related with cloud/snow discrimination, Bormann et al. (2012a) performed a manual inspection of all MODIS images to identify those where clouds were present. From a total of 2871 daily images between 2000 and 2010, only those images associated with clear-sky conditions were consider in the MOD-MADI dataset (a total of 358) leading to an average of about 32 images per snow season (May to early November). MOD-MADI snow cover is provided using a binary snow absence/presence algorithm at a resolution of 500 m. Data are available over a region that includes parts of New South Wales and Victoria over a regular grid of 745 latitudes by 897 longitudes. More specifically, the region encompass latitudes between − 34.6 and − 38.0°S and longitudes between 145.0 and 149.9 °E (see coloured grid points in Fig. 1b).

The MOD-MADI snow cover dataset was evaluated using 30-m Landsat true colour image composites on 15 clear-sky days (Bormann et al. 2012a). The evaluation showed that MOD-MADI underestimates total snow cover areas over the Australian Alpine region by about 13% and this is partially due to the influence of fractionally covered pixels (pixels with less than 50% snow cover) that are disregarded in MOD-MADI due to its binary nature. The negative bias related with the effect of fractionally covered pixels increases in areas where the proportion of marginal snow is greater.

2.2.2 MODIS-Th dataset

The second product is the one developed by Thompson (2016) (hereafter denoted as MODIS-Th). This dataset uses the MODIS level-2 daily reflectances from collection 5. The snow detection is performed using the well known Normalised Difference Snow Index (NDSI; Riggs et al. 2006) algorithm combined with the Normalised Difference Vegetation Index (NDVI) to identify snow-cover in forested areas (Thompson 2016). The NDSI algorithm is calculated using the normalised difference of two bands (one in the visible and one in the near-infrared). The NDSI has been used extensively in the literature to detect snow in various regions around the world (e.g., Crane and Anderson 1984; Hall et al. 2002). This product uses the automated ICLM algorithm of Thompson et al. (2015) to discriminate between snow and clouds. As such, the discrimination between snow and clouds is performed by an objective algorithm and does not depend on the skill of the analyst as in Bormann et al. (2012a).

MODIS-Th data are provided at a resolution of 500 m as a binary product only for grid points with an elevation higher than 1200 m (see coloured grid points in Fig. 1c). MODIS-Th region is thus smaller and comprised within the MOD-MADI region. In this study we use a gap-filled version containing daily values of snow cover for the period 2000–2014 (only from May to October included). The gap-filled version was derived by assuming that the detected snow persisted between observations unless the no-snow cover type was detected. Averaged across the region and the whole period, snow was detected in 6.2% of the days, clouds in 31.7%, no-snow in 32.1% with about 30.0% of missing values. The impact of using the gap-filled version is briefly discussed in Sect. 5.

2.3 Regional climate model ensemble

RCM simulations used in this study were performed in the context of the NARCliM project. The NARCliM project was designed to create regional scale climate projections for use in climate change impacts and adaptation studies, and ultimately to inform climate change policy making (Evans et al. 2014). In the following we provide a brief description of the NARCliM experimental set up. More details can be found in Evans et al. (2014) and on the University of New South Wales website (http://www.ccrc.unsw.edu.au/NARCliM/) and the AdaptNSW website (http://www.climatechange.environment.nsw.gov.au/Climate-projections-for-NSW/About-NARCliM/).

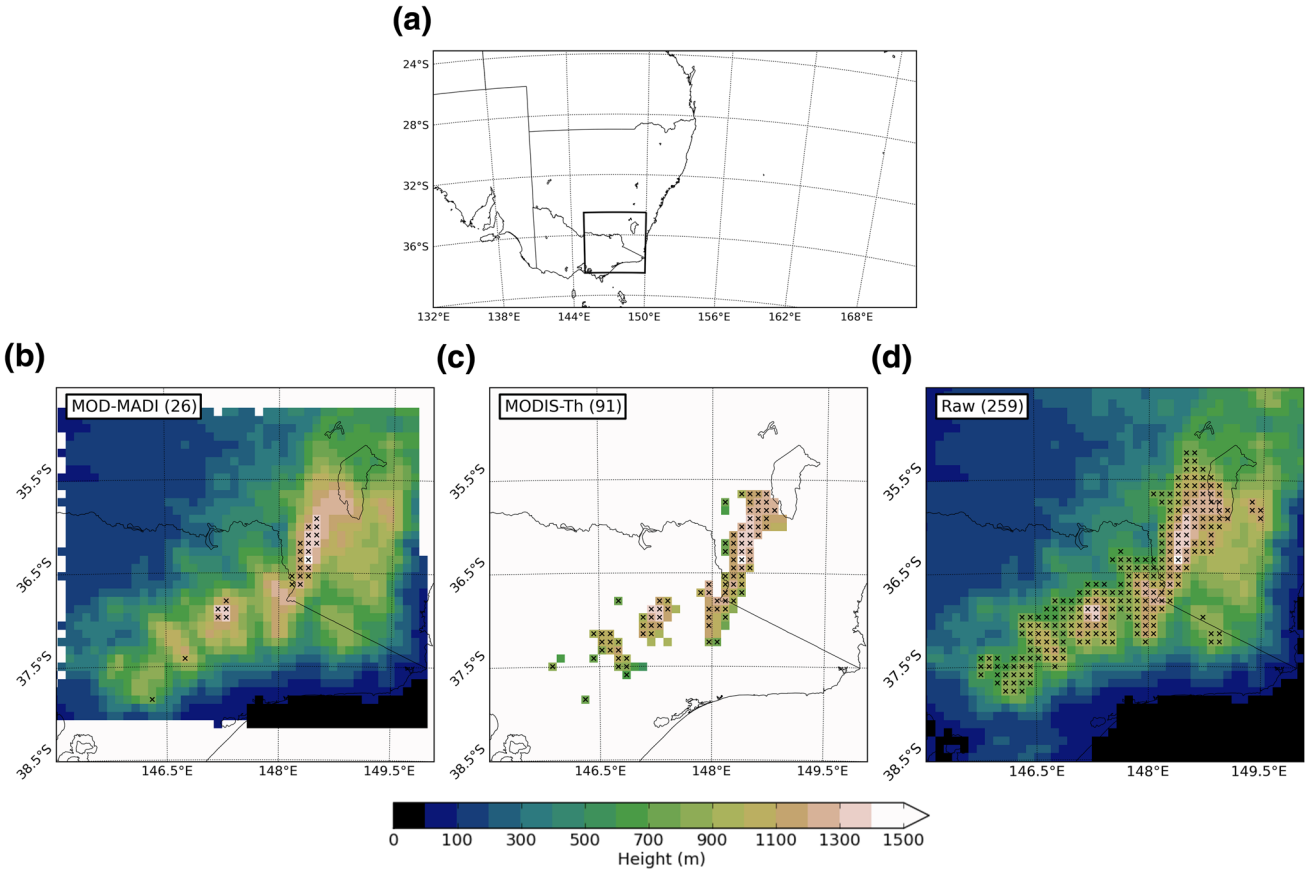

Fig. 1 The domain of the 10-km grid spacing NARCliM simulations and the region of study are shown in **a**. Grid points where the seasonal maximum snow-cover fraction exceeds 0.1 in at least 75% of years are shown with black crosses for the MOD-MADI (**b**), the MODIS-Th (**c**) and the NARCliM ensemble mean (**d**) datasets. The 10-km model elevation field is shown in colours only in those grid points where data is available for each dataset

The RCM ensemble has been created by selecting four GCMs from the 3rd Coupled Model Intercomparison Project (CMIP3) and downscaling each of these with three different configurations of the Weather Research and Forecasting (WRF) model. The GCMs were selected based on their skill in representing the climate over southeast Australia, their model independence and on the availability of the GCM outputs required as inputs to the RCMs. The independence was measured using the method developed by Bishop and Abramowitz (2013) based on the covariance of model errors as the basis for model independence. Additionally, the GCMs were chosen so that they covered as much as possible the future temperature/precipitation change space of the full CMIP3 multi-model dataset. The following four GCMs were selected: MIROC3.2-medres, ECHAM5, CCCMA3.1, and CSIRO-Mk3.0. For a more detailed discussion on the selection of GCMs the reader is referred to Evans and Ji (2012a).

The three different RCM versions were constructed using version 3.3 of the WRF model (Skamarock et al. 2008) by combining different surface/planetary boundary layer, cumulus and atmospheric radiation schemes. All three versions share the dynamical core, the Unified Noah land surface model (LSM) and the subgrid scale representation of microphysical processes (WDM-5 scheme). These three WRF versions were selected from a 36 member multi-physics ensemble based on their model skill and independence in a two-step selection process (Evans and Ji 2012b; Evans et al. 2014). First, individual members of the full multi-physics ensemble were evaluated over southeast Australia in order to remove from the ensemble those configurations that were not able to adequately simulate the climate. Second, from the subensemble obtained in the former step, a subset was chosen such that each selected member is as independent as possible from the others using Bishop and Abramowitz (2013) approach. Indeed, selected WRF versions correspond to three of the most independent/best performing models of the 36-member ensemble.

NARCliM simulations were carried out using a double-nesting approach where the GCMs are used to drive the RCM at 50-km grid spacing over a domain that covers the CORDEX-Austral Asia region (RCM50; see Fig. 1 in Evans et al. 2014), and then the RCM50 is used to

drive the same RCM with an horizontal grid spacing of 10 km over a domain that includes the Australian Alpine region (see domain in Fig. 1a). Only results from the 10-km resolution simulations are used in this study. All simulations were performed for three 20-year periods: present (1990–2009), near future (2020–2039), and far future (2060–2079) with future runs following the A2 scenario from the Special Report on Emissions Scenarios (SRES) (Nakićenović et al. 2000). The SRES A2 scenario assumes a very heterogeneous world, with continuously increasing global population and region-specific levels of economic growth, representing a high emissions scenario. According to Rogelj et al. (2012), the ensemble-median projected temperature change for the period 2090–2099 is 3.9 °C for the SRES A2 with a 66% intermodel range of [3.2,4.8] °C. These projections appear to be in between those resulting from the more recent 6.5 and 8.5 representative concentration pathways (RCP) that lead to an ensemble-median of ~ 2.9 and ~ 4.6 °C respectively for the same period.

The NARCliM ensemble provides a number of atmospheric and surface variables, most of them available at a 3-hourly frequency and a few variables (e.g. precipitation and temperature) available at an hourly frequency. NARCliM provides several snow-related variables including the liquid equivalent accumulated snowfall and several snowpack characteristics including snow depth, snow water equivalent and snow cover, all calculated within the Unified Noah LSM (shared by all NARCliM members). Within the LSM, the snowpack (e.g., snowpack water equivalent) can increase either when the fraction of frozen precipitation (snow/graupel) is greater than half the total precipitation, in which case it is assumed that all precipitation is solid, and/or when precipitation occurs over an effective skin temperature that is lower than or equal to 0 °C, in which case it assumed that all the precipitation will freeze at the surface. The snowpack can also decrease due to melting (when effective skin temperature is greater than 0 °C) or sublimation.

The snow cover fraction is the ratio of surface area covered by snow within a grid box (i.e., values range from 0 to 1) and is dependent upon the snow water equivalent and the vegetation type (Chen and Dudhia 2001; Ek 2003). For example, a grid box with forest (cropland) is considered to be fully covered by snow whenever the snow water equivalent is greater than 0.08 m (0.04 m). The snow depth contains the physical depth of the snowpack and is calculated from the snowpack water equivalent and its density that is governed via a time-dependent snow compaction algorithm (Ek 2003).

3 Snow seasonal descriptors and area of study

Simulated and satellite products are available at different spatial (500 m Vs. 10 km) and temporal (daily Vs. 3-hourly) resolutions. In order to compare the model output with MODIS-derived satellite observations, it is necessary to remap and resample the data to a common grid and temporal frequency. In this study, as similarly done by Kotlarski et al. (2014) and Da Ronco et al. (2016), the coarser grid has been used as the reference grid and the MODIS-derived products have been upscaled to the NARCliM grid mesh. Following Da Ronco et al. (2016), the upscaling is performed by simply averaging values from the 500-m resolution MODIS-derived data within 10-km RCM grid boxes (i.e., every RCM grid box comprises nearly 400 MODIS observed values). Only those 10-km grid boxes with at least 20% of valid data (i.e., about 80 grid points) are considered in the analysis. MOD-MADI and MODIS-Th datasets provide snow cover as a binary product: 0 (no snow) and 1 (fully covered). As a consequence, the upscaled snow cover fraction takes values between 0 and 1. As MODIS-derived datasets are available on a daily basis, simulated data were upscaled to the daily time scale by simply averaging over hourly and/or 3-hourly values.

The assessment of snow cover characteristics and future changes is performed based on the estimation of snow cover seasonal descriptors. Following Thompson (2016), for each season (i.e., from May to October included) we calculate seasonal mean and maximum snow cover together with the snow cover onset and melt days, and the seasonal snow cover duration:

- *Mean snow cover fraction* (*SCF*) corresponds to the seasonal averaged snow cover fraction at each grid point calculated using all available daily values. Units are in area fraction.
- *Maximum snow cover fraction* (*MxSCF*) corresponds to the maximum daily snow cover fraction of the season at each grid point. Units are in area fraction.
- *Snow cover onset day* (*SCOD*) corresponds to the first day of the season when the daily snow cover fraction is higher than 10%. In order to avoid ephemeral snow cover episodes (Thompson and Lees 2014), a 10-day moving average is applied to the daily snow cover time series before searching for the onset day. The onset day is given in day of the year (DOY) units (i.e., number between 0 and 365).
- *Snow cover melt day* (*SCMD*) corresponds to the last day of the season when the daily snow cover fraction is over a threshold of 10% at each grid point. Similar to SCOD, a 10-day running mean is applied to the daily time series before its calculation. Units are in DOY.

- *Snow cover duration* (*SCD*) corresponds to the duration of the snow cover and is determined as the difference between the onset day and the melt day. Units are in days (i.e., number between 0 and 365).
- *Mean snow cover extent* (*SCE*) the area covered by snow averaged over the snow season. Units are in 10^2 km^2.

The study area is located over southeast Australia and corresponds to an area of roughly 2° by 3° in latitude and longitude respectively (see Fig. 1a) with a maximum elevation of 1430 m near Mount Kosciuszko according to the 10-km resolution topography. Regular snow cover is limited to grid points located at relatively high elevations. Grid points with regular snow cover are here defined as those grid points where the seasonal SCD is larger than 1 day in at least 75% of the common period 2000–2009 (i.e., at least 8 years out of the 10 available). Black crosses in Fig. 1b–d show the resulting grid points for the MOD-MADI (Fig. 1b), the MODIS-Th (Fig. 1c) and the NARCliM ensemble mean (Fig. 1d) datasets. Figure 1b–d show that the number of grid points varies depending on the dataset considered and different areas are obtained by applying the above criteria to observed and simulated datasets. Specifically, the MOD-MADI satellite product shows that only 26 grid points are regularly snow covered while the MODIS-Th shows 91 and the NARCliM ensemble has 259 grid points for the common 2000–2009 period.

The period of study also depends on the data being considered. As already mentioned, MOD-MADI satellite observations are only available between 2000 and 2010 while MODIS-Th data are available between 2000 and 2014. Present climate RCM simulations are available between 1990 and 2009. As such, the evaluation of RCM simulations using satellite data is performed over the common period between 2000 and 2009. Near and far future changes are estimated using the full 20-year long simulations by comparing results from the present period (1990–2009) with near/far future periods (2020–2039 and 2060–2079 respectively).

4 Snow sensitive bias correction

This section provides a description of a methodology developed to produce a new set of bias corrected snowpack characteristics and includes four main steps. First, the parametric quantile mapping technique is applied to correct NARCliM simulated temperature fields. Second, using corrected temperatures, the Ruddell approximation (Ruddell et al. 1990) is used to separate the total precipitation in snow and rain contributions. Third, the parametric quantile mapping technique is applied to correct independently rainfall and snowfall fields as obtained from the Ruddell separation. Finally, the new corrected fields (minimum and maximum temperatures and Ruddell-derived snowfall rates) are used to force a temperature based snow melt/accumulation model that provides new estimations of snow depth and snow water equivalent at the surface.

4.1 Discriminating between rain and snow

A large number of studies have developed methods to estimate daily snowfall from the total precipitation and associated temperature records (Auer Jr. 1974; Ruddell et al. 1990; Dai 2008; Kienzle 2008; Ye et al. 2013; Frei et al. 2017). Over the Australian Alps, the dependence that precipitation type has on surface temperatures was studied by Ruddell et al. (1990) using over 16,000 days of daily temperature, precipitation and occurrence of snowfall from seven Australian alpine locations. The fraction of precipitation falling as snow from Ruddell et al. (1990) data is shown by the black crosses in Fig. 2. In order to use Ruddell results to separate snow/rain in observations and simulations, an analytical formula has been fitted to the data (see blue line in Fig. 2):

$$SF = a \cdot arctan(b \cdot (T_{min} - c)) + d \quad (1)$$

where SF and T_{min} denote the daily snow fraction and daily 2-m minimum temperature respectively. The best fit was obtained using the following parameters: $a = -0.363$, $b = -1.3$, $c = -1.421$ and $d = 0.493$. Using daily snow fractions as calculated from Eq. 1, we estimate daily snow and rain fields for each NARCliM simulation and the AWAP observations.

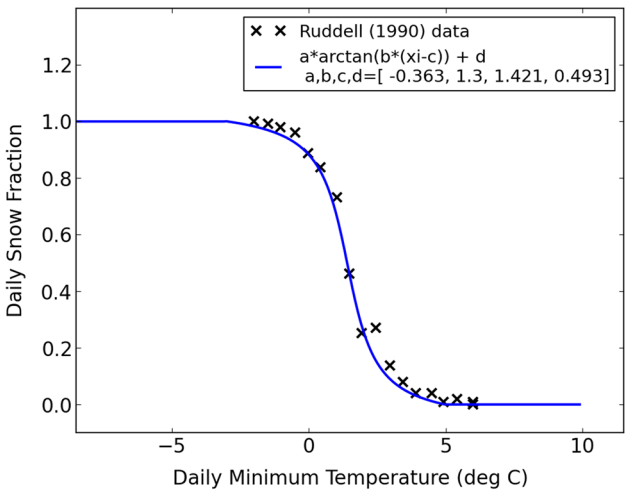

Fig. 2 Fraction of the total precipitation falling as snow as derived from observations (black crosses, data from Ruddell et al. 1990) and as fitted using Eq. 1 (blue line)

4.2 Correcting temperature, rain and snowfall fields

Bias correction (BC) techniques aim at correcting the raw output from climate models by using model errors that were identified with the aid of observations. As such, BC techniques can only be applied to those variables for which reliable observations are available. Over the region and period of analysis, daily observations are available only for minimum and maximum 2-m temperatures and total precipitation (see Sect. 2.1). Using the Ruddell approximation, rain and snowfall rates can also be obtained and used to directly correct the simulated rain and snowfall from the models.

In a recent paper, Frei et al. (2017) developed a methodology to correct simulated snowfall rates by independently correcting 2-m temperature and total precipitation fields that were used to derived snowfall rates. Their precipitation correction was performed by introducing an elevation-dependent correction factor that was assumed to vary linearly with height. Temperature fields were corrected by adding a constant value for which the spatially and temporally averaged simulated snowfall amounts matched the respective observation-based amount.

In this study we make use of the more sophisticated (and more computationally demanding) quantile mapping (QM) method using theoretical functions (see Piani et al. 2010; Argüeso et al. 2013a and references therein) to adjust both temperature and precipitation fields. The QM method is a distribution-based approach that corrects raw output values so the simulated quantiles converge towards the observed ones. This method does not only correct the mean bias but also higher moments (e.g., 99th percentile), an important requirement when dealing with hydrological impact studies. Previous works, notably the work by Gudmundsson et al. (2012) and Ivanov and Kotlarski (2016), identified QM as one of the best-performing BC methods with respect to both bias correcting and downscaling of RCM output to the site scale. Both studies also showed "no advantage of the parametric over the empirical QM methods" although when dealing with future climate corrections the parametric method is preferred as it allows for a more consistent correction of values that are outside the range of present-day (training) values.

The first step in applying the quantile mapping method is to fit theoretical distributions to the time series of the variable of interest. This fitting is performed independently at every grid point. For temperature variables, we assume that the probability distribution of both observed and simulated daily minimum or maximum 2-m temperatures is approximated by a Gaussian probability density function.

Precipitation corrections are also performed using the quantile mapping approach. Corrections are performed independently for the total precipitation and the Ruddell-derived rain and snowfall. The explicit distinction between the solid and liquid phases in the correction process is justified by the fact that snowfall and rainfall distributions are generally significantly different. For all precipitation variables, we assume that the probability distribution of both observed and simulated daily precipitation rates can be approximated using a gamma probability density function. As for temperature, the fitting is performed independently at individual grid points. Following Argüeso et al. (2013b), the parameters of the gamma distributions are calculated using only wet days, which are defined as days with precipitation above a certain threshold. Here we define any day in the AWAP dataset with precipitation larger than 0.2 mm as wet. Modelled wet days are defined in a more flexible way, using a calibrated precipitation threshold as proposed in Schmidli et al. (2007) to adjust the potential excess of wet-day frequencies and thus provide a better estimation of the corrected accumulated values.

All fits are calculated on the present day simulation (1990–2009) using daily distributions from the whole year (not only the snow-season). When corrections are extrapolated into the future, they rely on the stationarity assumption of the model biases (Maraun 2012; Bellprat et al. 2013).

4.3 Snow melt/accumulation model

The snow melt/accumulation model used here is the model described as Scheme 1 in Bormann et al. (2014). It is a temperature index model that explicitly accounts for the unusually high snow densities (and large interannual changes in density) found in the Australian snowpack. The snow melt/accumulation model uses daily snow rates and minimum and maximum temperatures from the BC output. It also uses variables characterising the landscape such as the elevation, latitude and mean potential relative radiation in order to estimate the snow density at each grid point and for each day of the year. As the snow model is run at the 500 m resolution, the 10-km BC fields need to be interpolated to the 500-m grid mesh.

For temperature fields, the interpolation is performed using a bilinear approach combined with a correction to account for the elevation dependence of 2-m air temperatures. More specifically, the elevation correction is performed by adding the difference between the high-resolution and low-resolution topography fields multiplied by the middle-latitude standard atmosphere lapse rate ($\Gamma = -6.5$ K km^{-1}). For snow fields, the interpolation is performed using simply a bilinear method.

Temperature-index models of snowmelt use 2-m air temperature as a proxy for constraining snowmelt and may be expressed generally as:

$$SM = \alpha \cdot (T_{mean} - T_{ref}) \tag{2}$$

where SM is the snowmelt rate (mm day^{-1}), T_{mean} is the 2-m daily mean temperature (°C), α is the melt parameter (mm °C day^{-1}) and T_{ref} is a reference temperature above which melt starts to occur and here is set to 0 °C. The melt parameter α is calculated as a function of varying snow density which accounts for both interannual climate variability and a difference between exposed and forested sites. More details are given in Bormann et al. (2014).

The snow melt/accumulation model outputs two characteristics of the snowpack: snow depth and snow water equivalent. The snow cover is then calculated using snow depth estimations by assuming:

- the grid box is fully covered by snow ($SC = 1$) when the snow depth is equal or higher than 250 mm;
- snow cover varies exponentially as $SC = 1 - \left[\exp\left(-S \cdot \frac{SD}{250}\right) - \frac{SD}{250} \cdot \exp(-S)\right]$ when the snow depth ranges between 0 and 250 mm.

with S a constant taken to be equal to 2.6. The 250 mm snow depth threshold used here is consistent with thresholds in the Unified Noah LSM (see Fig. 1 in Ek 2003). The snow cover calculation is performed at the 500 m grid mesh. All snowpack variables (snow depth, snow water equivalent and snow cover) are later remapped to the 10-km grid mesh in order to compare with the raw data.

5 Present-day snowpack in satellite observations

Figure 3a shows snow-season mean values and long term trends of the SC extent (SCE) over the common MODIS-Th area (black crosses in Fig. 1c) based on MODIS-Th (2000–2014) and MOD-MADI (2000–2010) satellite products. Over their common period, both products show similar interannual variability although the SCE in MODIS-Th is roughly twice as large as in MOD-MADI showing a large observational uncertainty. Both time series show similar negative tendencies with decreases of 220 and 180 km^2 per

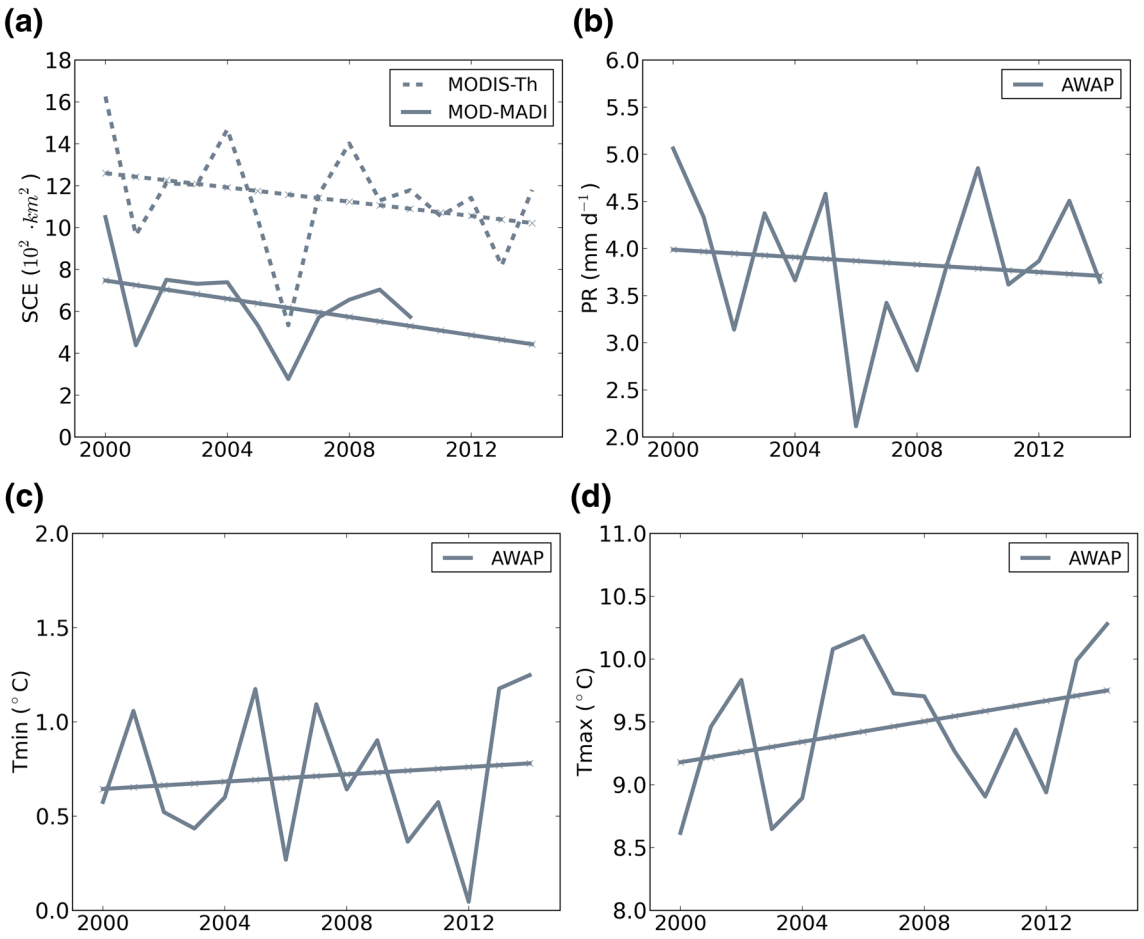

Fig. 3 Time series of snow-season average satellite-derived SCE (**a**), total precipitation (**b**), minimum temperature (**c**) and maximum temperature (**d**). Results are shown for the period 2000–2014. Areal averages were calculated using the MODIS-Th region. None of the trends appear to be significant according to a Mann-Kendall test at the 5% significance level ($p < 0.05$)

decade for the MOD-MADI and the MODIS-Th products respectively. None of these trends appear to be statistically significant according to a Mann-Kendall test at the 5% significance level largely due to the relatively short period of the analysis (11 and 15 years) combined with the large interannual variability.

The number of grid points with regular snow cover in both MODIS-Th and MOD-MADI products is also very different. While MODIS-Th leads to a total of 91 grid points, MOD-MADI only suggests 26 grid points. As mentioned in Sect. 2.2, it has been shown that MOD-MADI data underestimates observed snow cover using higher resolution Landsat images. According to Bormann et al. (2012a), MOD-MADI's underestimation is close to 15% and it is expected to be larger over areas with greater proportion of marginal snow cover. Assuming MODIS-Th as truth would imply that MOD-MADI underestimates snow cover by about 80%, nearly five times more than shown by Bormann et al. (2012a). It is thus unclear whether differences between both satellite products are only due to a MOD-MADI underestimation or to a combination of MOD-MADI underestimation with a MODIS-Th overestimation. As discussed in Section 1 in the Supplementary Material, annual differences between mean SCE do not appear to be related with the fact that MODIS-Th consists of a continuous (gap-filled) time series compared to the discrete nature of the MOD-MADI product.

Time series of seasonal-mean total precipitation and minimum and maximum temperatures for the period 2000–2014 from the AWAP dataset are shown in Fig. 3b–d (also averaged over the MODIS-Th region). The decrease in SCE appears to be related with positive trends in both minimum and maximum temperatures although mostly the later as the maximum temperature shows a much larger tendency (0.4 vs. 0.1 °C per decade) and a higher temporal correlation with the MODIS SCE (− 0.59 vs. − 0.08 for MODIS-Th and − 0.65 vs. 0.017 for MOD-MADI). While both trends are not statistically significant over the period 2000–2014, tendencies in snow-season maximum temperature appear to be statistically significant when the longer 1990–2014 period is considered (not shown). In agreement with these results, using in situ observations Fiddes et al. (2015) showed that maximum temperatures were more correlated with snow-related variables than minimum temperatures.

As shown by Nicholls (2005) using in situ measurements of snow depth, snowpack decreases can also be partly explained by the negative trend in total precipitation (− 0.15 mm day^{-1} per decade during 2000–2014) as SCE and total precipitation time series are moderately correlated (0.27 for MODIS-Th and 0.38 for MOD-MADI). While the trend in total precipitation appears to be statistically not significant for the period 2000–2014 this seems to be due to the short period as the trend is statistically significant when the longer 1990–2014 period is considered. The decrease in precipitation over the region (Nicholls 2005) was shown to be strong on the western slopes as well as at high elevations but weak in the eastern slopes of the Snowy mountains (Chubb et al. 2011). This general decrease has been associated to a weakening of the dominant westerly atmospheric flow in response to a strengthening of the belt of high pressures (Timbal and Drosdowsky 2013).

Figure 4 shows the spatial distribution of seasonal-averaged snow cover descriptors for the MODIS-Th product (MOD-MADI results are shown in Fig. S1 of the Supplementary Material). Mean snow cover fractions (Fig. 4a) vary between 0 and 0.7 and appear to show a moderate dependence with elevation with a spatial correlation of 0.42 (i.e. larger SC fractions at higher altitudes). Maximum SC fractions (Fig. 4b) are generally higher than 0.7 and reach values of 1 in many grid points. The comparison between results from MODIS-Th and MOD-MADI shows that while MODIS-Th data show significantly higher values than MOD-MADI for both mean and maximum SC fractions, spatial patterns are very similar with spatial correlations of 0.96 and 0.82 for SCF and MxSCF respectively.

According to the MODIS-Th product, a total of 91 grid points show regular snow cover (i.e. seasonal SCD larger than 1 day in at least 75% of the period). For this grid points, the mean snow fraction over the whole season is 0.13. The mean snow cover onset (Fig. 4c) occurs as early as 134 DOY (mid-May) and as late as 223 DOY (mid-August) and the mean end of the snow season (Fig. 4d) varies between 215 (early August) to 300 DOY (late October). This leads to a mean duration of the snow season that varies from a few days to nearly 165 days in the mountain peaks (Fig. 4e). As expected, snow cover descriptors are highly correlated with each other with high values of SC fractions, SC melt days and SC durations occurring simultaneously with low values of SC onset days. Areal-mean snow cover descriptors for the MODIS-Th and the MOD-MADI products are shown in Table 2.

6 Present-day snowpack in NARCliM simulations

In this section we focus our attention on the evaluation of the NARCliM ensemble to represent the snowpack and related variables over the Australian Alps. For a more general discussion about temperature and precipitation biases in the NARCliM ensemble the reader is referred to Olson et al. (2016) and Di Luca et al. (2016).

Figure 5 shows NARCliM ensemble mean biases compared with the satellite products for the various snow cover descriptors over the period 2000–2009. Biases in Fig. 5 are calculated by taking the minimum bias between the ensemble mean and the two satellite products (MOD-MADI or MODIS-Th). Moreover, the bias is set to zero if the ensemble

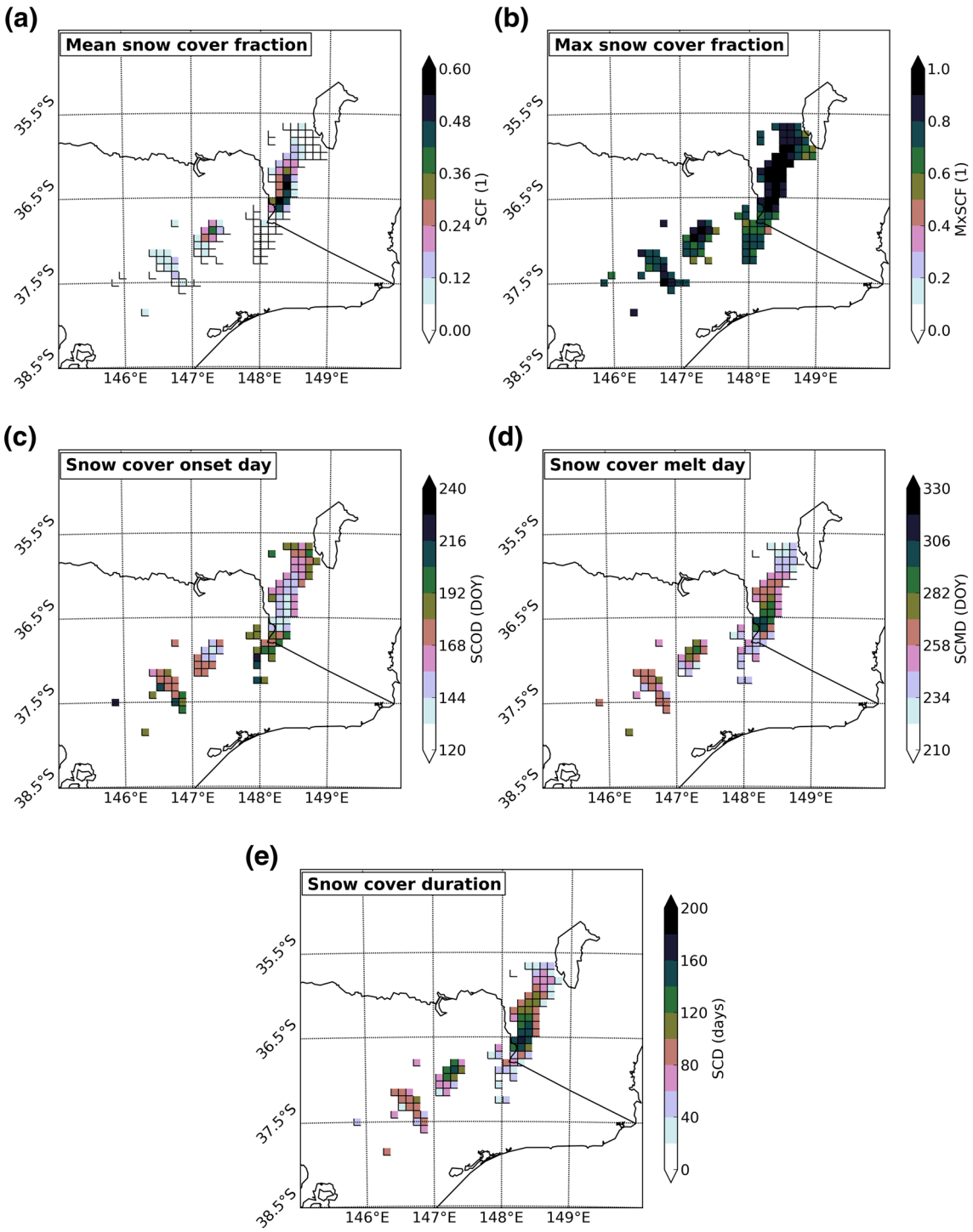

Fig. 4 Present-day (2000–2009) climatology of snow cover as derived using the MODIS-Th satellite dataset for the mean fraction (**a**), the maximum fraction (**b**), the onset day (**c**) and melt day (**d**) and the total duration (**e**). Mean and maximum fractions were calculated using the snow season period (May to October included)

mean falls within the observational range. This is an adoption of the method first proposed in Evans et al. (2016).

The NARCliM ensemble-mean biases are separated into three categories (a) less than half of the models show a significant bias (insignificant areas, ensemble-mean bias is shown in colour), (b) at least half of the models show a significant bias and at least 80% of significant models agree on the sign of the bias (significant areas of agreement,

Table 2 Mean SC fraction, onset day, melt day and duration for MODIS products and NARCliM raw and BC datasets

Data	SCF (1)	SCOD (DOY)	SCMD (DOY)	SCD (days)
MOD-MADI	0.071	192	261	69
MODIS-Th	0.13	172	253	81
NARCliM Raw	0.18	162	264	102
NARCliM BC	0.11	183	237	54

Results correspond to the common MODIS-Th area between 2000–2009

stippled with an slash ("|") symbol), and (c) at least half of the models show a significant bias and less than 80% of significant models agree on the sign of the bias (significant areas of disagreement, stippled with a cross ("x") symbol). Non-stippled areas thus indicate that biases are within the interannual variability and is the preferred outcome. Also, the lack of cross stippling indicates that among the models significant areas of disagreement are not widespread. For each variable (e.g., minimum temperature), the significance of biases of individual models was estimated with respect to the interannual variability using a Students t-test at the 5% significance level ($p < 0.05$). The use of t-tests implicitly assumes that observed and simulated annual mean values follow normal distributions.

The NARCliM ensemble mean tends to overestimate snow cover mean fractions compared with satellite observations in most of the Australian Alps and produces an underestimation over the highest peaks around Mount Kosciuszko. A total of 88 out of the 112 grid points over the Australian Alps (i.e. 79.5% of the MODIS-Th area) show biases that are significant and where models agree on the sign of the bias. There are also 6 grid points showing significant changes for which simulations do not agree on the sign, generally located in the transition between negative/positive biases.

Consistent with the general overestimation of the mean snow cover fraction, NARCliM simulations suggest a significantly longer snow season (Fig. 5e) due to both a too early start (Fig. 5c) and a too late finish (Fig. 5d) compared to the MODIS products. Table 2 shows areal-mean values over the regular snow covered grid points in the MODIS-Th region for the start, the end and the duration of the snow season. While the observational uncertainty is quite large, the snow season in the NARCliM ensemble mean starts about 10 days too early and ends nearly 10 days too late compared with the closest observation, leading to a bias of about 21 days in the mean duration. It should be noted that local biases are much larger than areal-mean values because there is some compensation in the averaging process (i.e. biases show a mix of positive/negative values). While the snow cover evaluation is carried out using a single 10-year period, mean biases as presented here are robust to sampling uncertainty related with interannual variability. For a more detailed discussion on this issue refer to Section 2 of the Supplementary Material.

The causes of the general overestimation in the NARCliM ensemble have to be related with either the amount of snow falling on the ground and/or the accumulation/melting of the snow at the surface. Top panels in Fig. 6 show the spatial distribution of mean temperature and total precipitation ensemble mean biases compared with AWAP observations over the period 1990–2009. Over most of the Australian Alps, the ensemble has a cold bias of about 2°C mainly due to a cold bias in the simulated maximum temperatures (not shown). This cold bias is not just a result of the ensemble mean but a robust feature across individual simulations as suggested by the comparison between monthly mean values in AWAP and the NARCliM individual simulations (see Fig. 6c). Ji et al. (2016) suggested that this cold temperature bias might be partly explained by the use of the Noah LSM that has been shown to overestimate total soil moisture content. It is unclear, however, whether this is still true in the presence of snow at the surface.

Figure 6b, d also show that the ensemble mean and most individual simulations overestimate the total precipitation compared with AWAP by about 2 mm day^{-1} over the whole region but attaining about 4 mm day^{-1} over the western slopes of the Australian Alps. As shown in Fig. S3 in the Supplementary Material, most of the overestimation in the total precipitation is related with an excess of snowfall as derived using the Ruddell approximation. As noted by Chubb et al. (2016), the AWAP product largely underestimates precipitation over the western slopes of the Snowy Mountains compared with an independent network of gauge data from Snowy Hydro Ltd and it is thus unclear to what extent NARCliM ensemble mean biases are accurate. However, the lack of a corrected version of the AWAP data over the mountains prevents us to properly address this issue.

Consequently, both temperature and precipitation errors in NARCliM simulations would contribute to produce an excess of snowfall over the Snowy Mountains and eventually a longer lasting snowpack due to the cold temperature biases. Using several RCMs, Frei et al. (2017) also found similar precipitation and temperature biases over the Swiss Alps suggesting that some of these biases might be related with a systematic misrepresentation of some snow-related process.

In order to gain more insight into the sources of the snow cover errors, a multiple linear regression analysis was performed independently in each grid point by using seasonal mean values. Averaged over the Australian Alps, the regression analysis shows that 55% of the seasonal-mean snow cover errors can be explained using minimum,

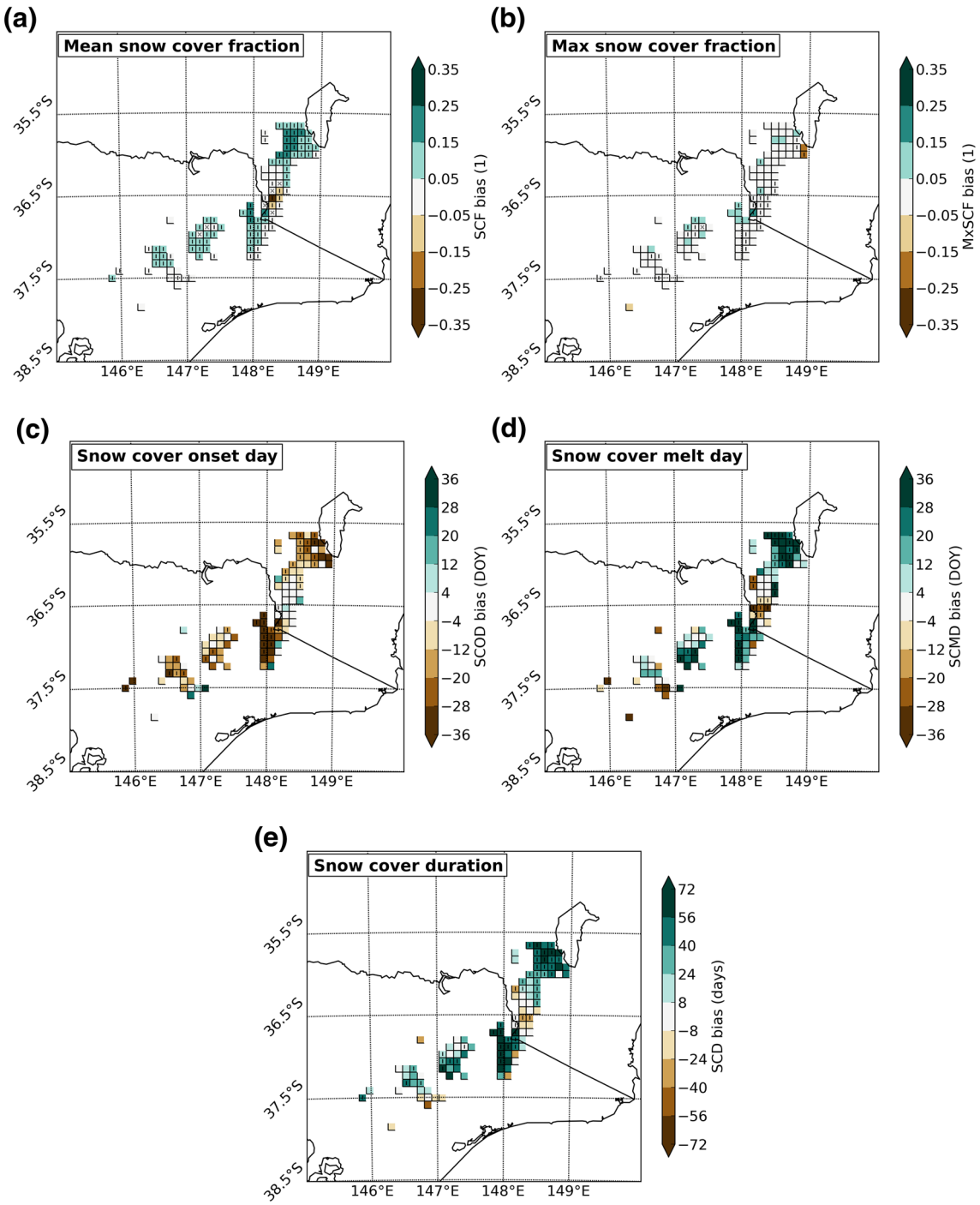

Fig. 5 NARCliM ensemble mean biases compared to the MODIS-derived datasets for present-day (2000–2009) snow cover descriptors. Biases are calculated with respect to the closest observation-based value (i.e., MOD-MADI or MODIS-Th) and set to zero if model outputs fall within the observational range. Significant areas of agreement are stippled with the "|" symbol (see Sect. in the text). Only results over the common MODIS-Th region are shown

maximum and total precipitation errors as predictors (see Table 3). Regardless of the simulation considered the largest errors in the snow cover arise from errors in the simulation of maximum temperature with a mean correlation coefficient across models of − 0.62 and relatively small variability between results from different simulations. As expected, the correlation coefficient between errors in snow cover and in total precipitation is always positive (an excess of precipitation leads to an excess of snow cover) with a mean value of 0.29 although there is a large range

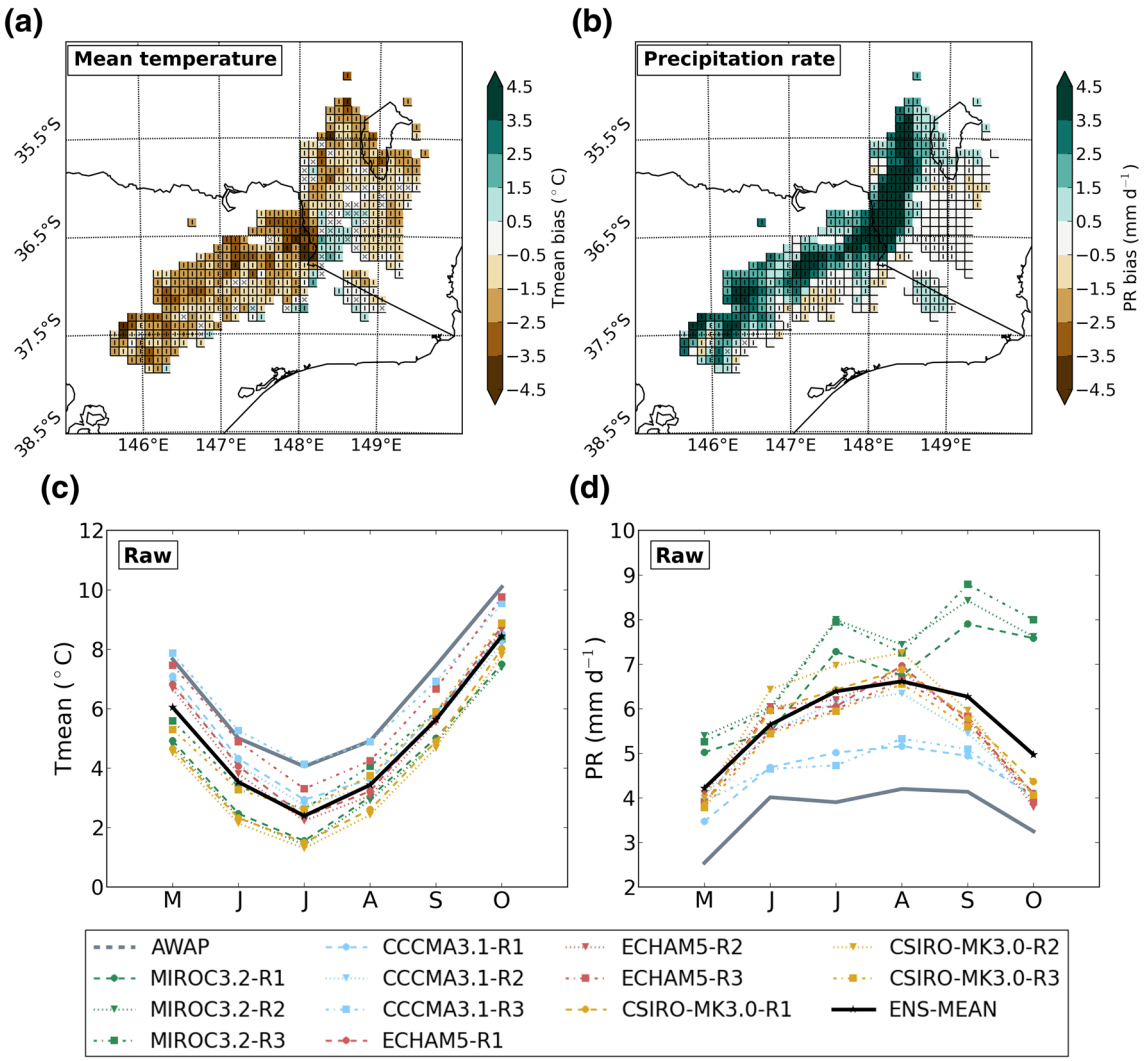

Fig. 6 Present-day (1990–2009) seasonal-mean biases (top panels) and monthly mean distributions (bottom panels) of mean temperature and total precipitation. Top panels show results for the ensemble mean and bottom panels include results for individual models and observations. Significant areas of agreement are stippled with the "|" symbol (see discussion in the text)

of responses among NARCliM members. This error analysis suggests that correcting temperature and precipitation fields prior to the application of a snow melt/accumulation model can provide significant improvements in the representation of the snowpack, supporting the use of a bias correction technique.

Following the steps described in Sect. 4, a bias correction methodology was applied by driving an independent snow melt/accumulation model with bias corrected temperature and precipitation fields. Figure S4 in the Supplementary Material presents temperature, total precipitation and snowfall mean biases using the BC NARCliM data. The BC is able to effectively eliminate most temperature and precipitation biases affecting the raw data and biases appear to be non-significant over most of the domain. Moreover, monthly mean values for individual simulations (right panels in Fig. S4) show that the BC methodology corrects the ensemble mean together with individual members.

Figure 7 shows the seasonal-mean biases of the BC snow-cover descriptors compared to MODIS-derived products. Over most of the Australian Alps, the BC data reduce snow-cover fraction biases relative to MODIS-Th with an overall mean bias of − 0.022 compared with a 0.052 obtained using the raw data (see Table 2). To avoid the compensation between positive and negative biases in the areal mean calculation we calculated the root mean square error. Compared to MODIS-Th data, the areal-mean root mean square error is 0.12 for the raw data and 0.069 for the BC data thus showing that local errors are reduced by a factor of two. The area of the Australian Alps were the ensemble mean biases are significant decreases substantially from 79.5% in the raw data to 14.3% in the BC data (using the MODIS-Th

Table 3 Areal-mean temporal correlation between seasonal-mean snow cover errors (SC^{err}) and the three predictors: total precipitation (PR^{err}; first column) and maximum (T^{err}_{max}; second column) and minimum (T^{err}_{min}; third column) temperatures for individual simulations and the ensemble mean

	$\overline{r(SC^{err}, PR^{err})}$	$\overline{r(SC^{err}, T^{err}_{max})}$	$\overline{r(SC^{err}, T^{err}_{min})}$	$\overline{R^2}$
MIROC3.2-R1	0.38	− 0.59	− 0.09	0.44
MIROC3.2-R2	0.51	− 0.67	0.1	0.59
MIROC3.2-R3	0.59	− 0.64	0.21	0.54
CCCMA3.1-R1	0.2	− 0.58	− 0.41	0.52
CCCMA3.1-R2	0.11	− 0.57	− 0.4	0.52
CCCMA3.1-R3	0.13	− 0.45	− 0.28	0.43
ECHAM5-R1	0.34	− 0.67	− 0.35	0.58
ECHAM5-R2	0.4	− 0.72	− 0.4	0.63
ECHAM5-R3	0.38	− 0.65	− 0.23	0.6
CSIRO-MK3.0-R1	0.04	− 0.62	− 0.31	0.56
CSIRO-MK3.0-R2	0.18	− 0.68	− 0.24	0.62
CSIRO-MK3.0-R3	0.2	− 0.58	− 0.14	0.54
NARCliM Mean	0.29	− 0.62	− 0.21	0.55

Last column shows the total variance explained by the full multi linear regression. The areal mean is calculated using the MODIS-Th region and only data from the common 10-year period (2000–2009) are used. Note that the sum of individual factors does not add to the total variance as the factors are correlated

common area). The BC data largely improves the spatial distribution of snow compared to the raw simulation. The spatial correlation coefficient between the mean SC fraction in the raw ensemble mean and observations is 0.65 and 0.64 for the MOD-MADI and MODIS-Th respectively while it increases to 0.91 and 0.90 when using the BC dataset. The corrected snow cover performs very well in most of the domain although it tends to somewhat overestimate SC fraction in grid points surrounding Mount Kosciuszko where the raw data produce a significant underestimation.

Table 2 shows areal-mean values over the regular snow covered grid points in the MODIS-Th region for the start, the end and the duration of the snow season for the raw and BC datasets. Contrary to the raw data, the duration of the snow season in the BC data tends to be too short compared to both MODIS datasets largely due to a much earlier melt of the snowpack compared datasets. This might be related with either somewhat low values of snowfall and/or the snow melt being too strong.

Figure 8 shows monthly mean SC extent, snow water equivalent and snow depth for MODIS-observations (only for snow cover) and both the raw (left panels) and BC (right panels) datasets. For all snowpack variables, the monthly-mean annual maxima tends to occur later in the BC compared to the raw data. This seems to be an improvement when looking at the MODIS-derived annual cycle (Fig. 8a, b) but also considering the annual cycle as observed using in situ snow depth measurements (e.g., Hennessy et al. 2008; Bhend et al. 2012).

Regardless of the snowpack variable considered, the spread across simulations is largely reduced in the BC data compared with the raw data. This result is expected as the correction towards observations reduces differences across the input parameters (e.g., temperature and snowfall) driving the snowpack model. The spread is generally explained by both the choice of the GCM (i.e., lateral boundary conditions) and the choice of the RCM (i.e., subgrid-scale processes representation). Specifically, simulations performed with version WRF-R2 tend to show the largest snow cover extents, particularly when driven by CSIRO-MK3.0 and MIROC3.2 while WRF-R3 simulations show the smallest differences. The dependence of biases on the choice of the RCM are clearly related with their representation of near-surface temperatures with WRF-R3 simulations showing the warmer temperatures and WRF-R2 the coldest values (see Fig. 6c).

It is also interesting to note that while monthly mean SC extent is much larger in the raw than in the BC data, differences between snow water equivalent and snow depth are much smaller between both datasets. This results from differences in the spatial distribution of the snow water equivalent. The BC output tend to show deeper snow depths (and more snow) over high elevation grid points but shallower depths (and less snow) elsewhere (see top panels in Fig. S5 in the Supplementary Material). These differences in the spatial distribution of the snowpack tend to favour a larger snow cover extent in the raw data. Also, some differences arise because both snowpack models (the Noah LSM used within the NARCLiM raw simulations and the temperature-index model used with the BC data) lead to different values of snow depths for a given amount of snow water equivalent. Specifically, the Unified Noah LSM associates higher depths than the BC snowpack model for a given snow water equivalent value. Differences between both snowpack models are ultimately related with the estimation of the snow density and its temporal evolution through the season. The scatter plots in bottom panels in Fig. S5 in the Supplementary Material show a clear linear relation between snow water and snow depth for both datasets but the slope, proportional to the snow density, is significantly larger in the raw data.

7 Future changes in NARCliM simulations

This Section discusses the projected future changes in the alpine climate using the raw and BC NARCliM datasets. For the sake of brevity, we only discuss in detail far future

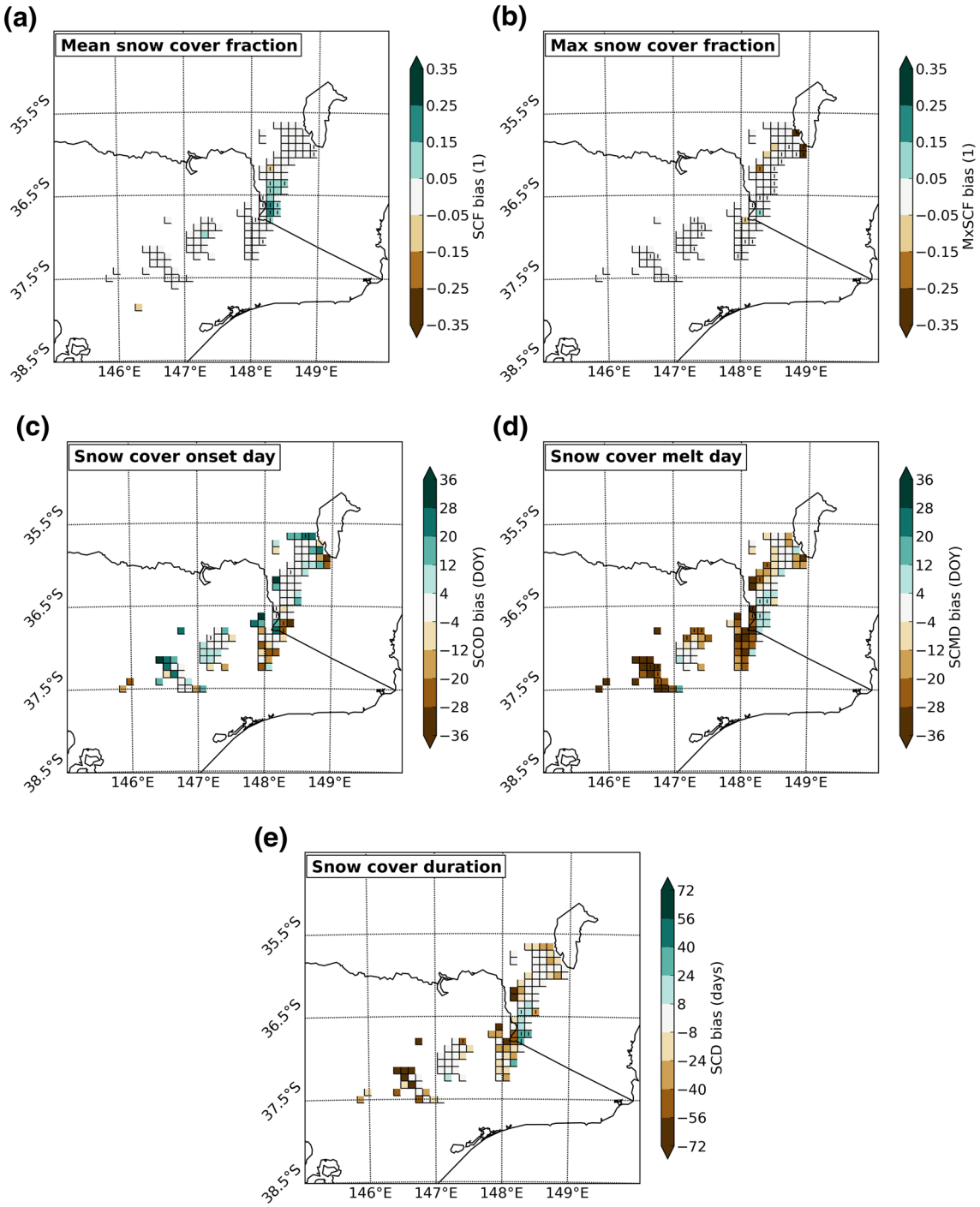

Fig. 7 Bias corrected NARCliM ensemble mean biases compared to the MODIS-derived datasets for present-day (2000–2009) snow cover descriptors. Biases are calculated with respect to the closest observation-based value (i.e., MOD-MADI or MODIS-Th) and set to zero if model outputs fall within the observational range. Significant areas of agreement are stippled with the "|" symbol (see discussion in the text). Only results over the common MODIS-Th region are shown

(2060–2079) changes compared with present climate (1990–2009). Near future (2020–2039) projections are only summarised as they are qualitatively similar to far future projections. A more general discussion about future changes in temperature and precipitation as projected by the NARCliM ensemble can be found in Olson et al. (2016).

Figure 9 shows the NARCliM ensemble mean far-future changes compared with present-day values for mean temperature (left panels) and total precipitation (right panels).

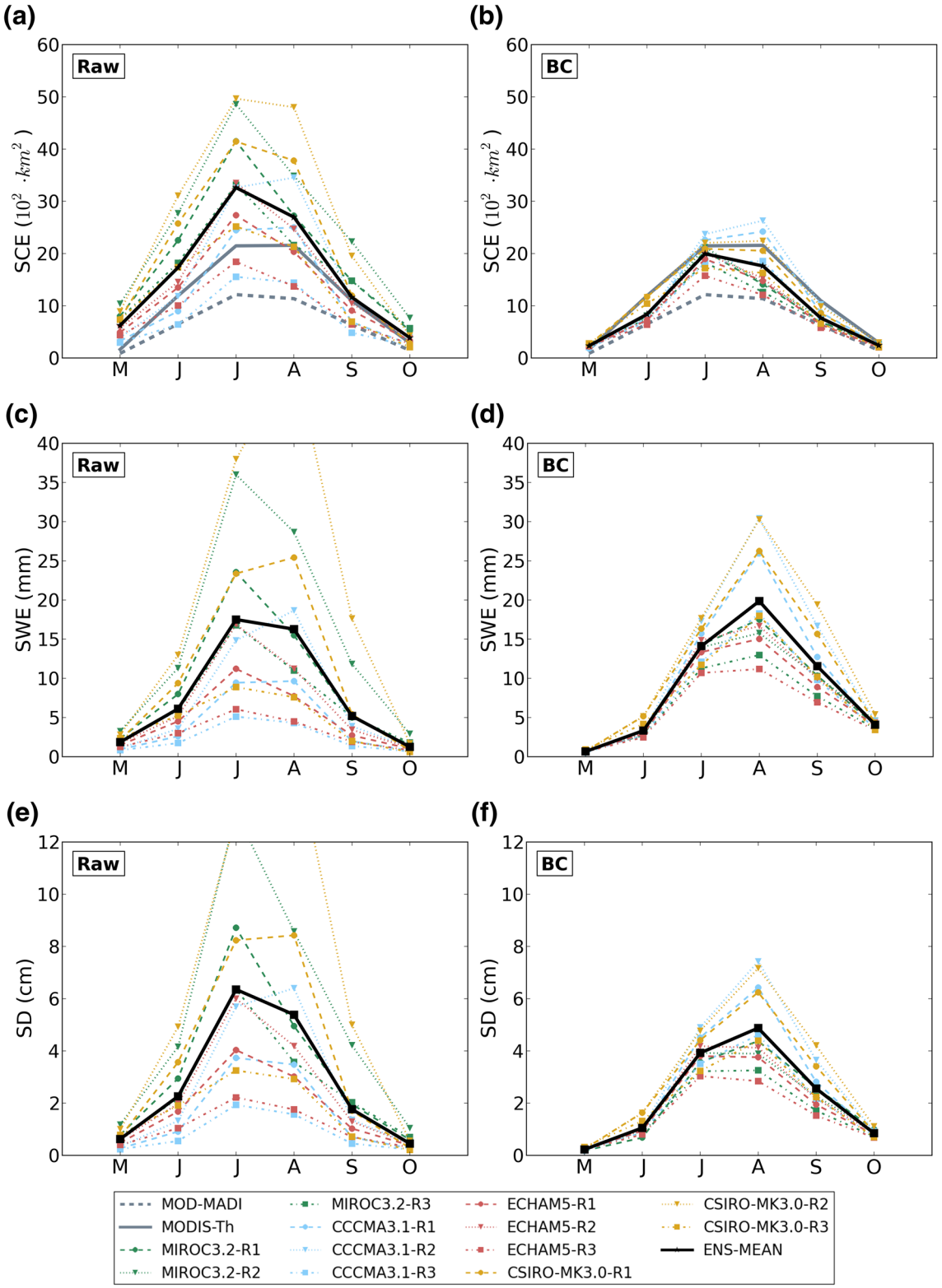

Fig. 8 Monthly mean snow cover extent (top panels), snow water equivalent (middle panels) and snow depth (bottom panels) from each NARCliM ensemble member, the ensemble mean and the MODIS products (when available). Results from the raw (left panels) and the BC (right panels) NARCliM datasets are shown for the period 2000–2009. Areal-mean values were calculated using the common MODIS-Th area (see Fig. 1c)

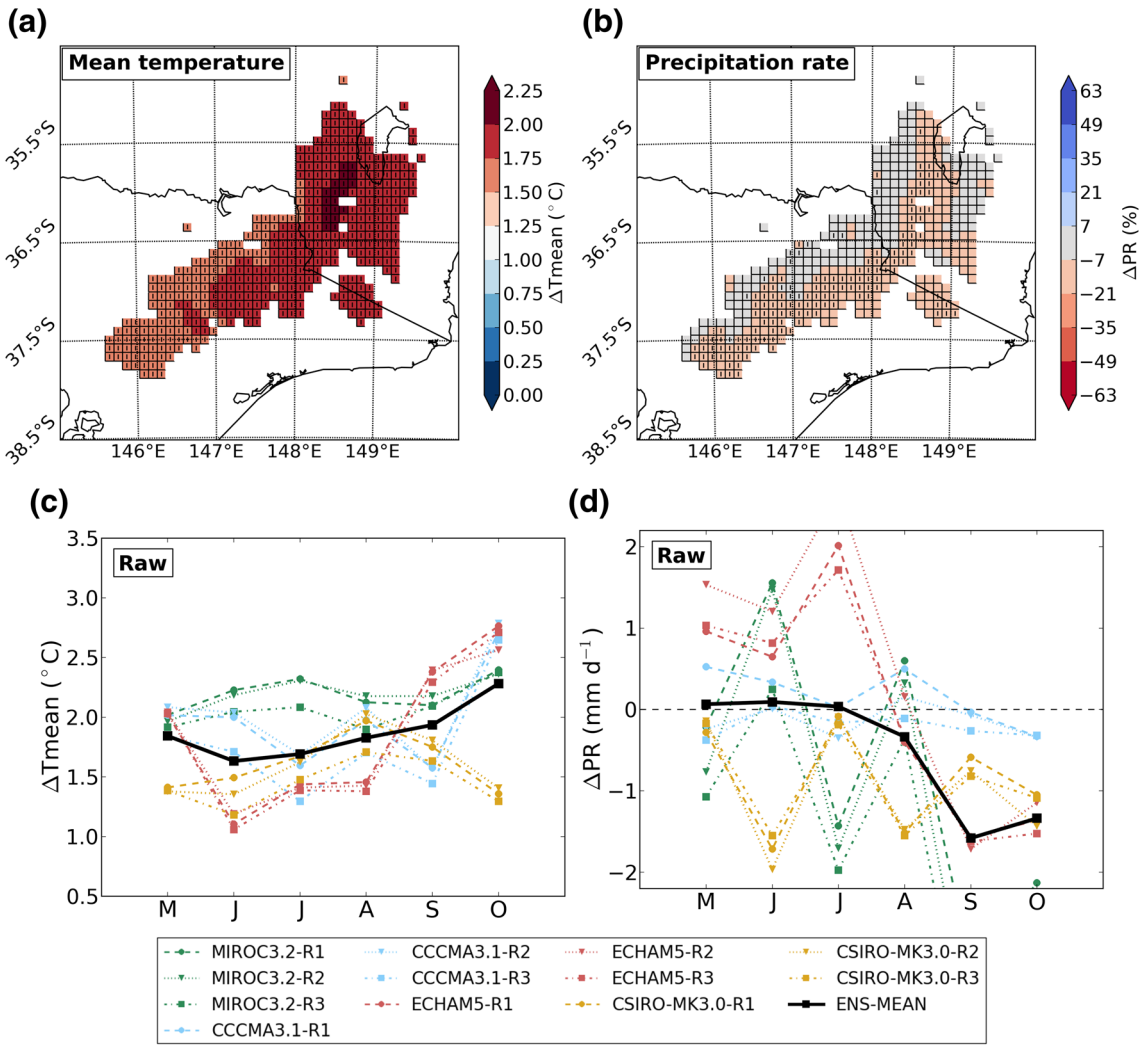

Fig. 9 Far-future (2060–2079) projected changes for mean temperature (left panels) and total precipitation (right panels) compared to the present-day (1990–2009) climatology. Top panels show results for the spatial distribution and bottom panels for the seasonal cycle. Monthly mean values were calculated by averaging over grid points that have regular snow cover in all three periods

The stippling in top panel plots indicates the level of model agreement about future changes. As done with the "biases significance", the NARCliM ensemble-mean changes are separated into three categories (a) less than half of the models show a significant change (insignificant areas, ensemble-mean change is shown in colour), (b) at least half of the models show a significant change and at least 80% of significant models agree on the sign of the change (significant areas of agreement, stippled with a slash ("/") symbol), and (c) at least half of the models show a significant change and less than 80% of significant models agree on the sign of the change (significant areas of disagreement, stippled with a dot ("x") symbol). Non-stippled areas thus indicate that changes are within the interannual variability. The significance of changes of individual RCM-GCM pairs was estimated with respect to the interannual variability using a Students t test at the 5% significance level ($p < 0.05$) assuming equal variances for the observed and simulated time series. The use of t tests essentially assumes that annual mean values follow a normal distributions in past and future periods.

Figure 9a) shows that the warming trends observed in the current climate will continue in the future with significant warming everywhere over the Australian alpine region. Averaged across raw simulations, far future mean temperature changes vary between 1.7 and 2.1 °C (areal-mean value of 1.9 °C) with larger changes for maximum than for minimum temperatures (see Fig. S6 in Supplementary Material). These future changes are slightly smaller to those found by Grose et al. (2015a) (see their Fig. 4.2.4) using output from 39 GCM simulations from the CMIP5 database that were performed following the RCP8.5. Note that in Grose et al. (2015a) the region of analysis and the

base period are different than in our study thus preventing a direct comparison. Also note that, as mentioned before, the RCP8.5 leads to higher temperature increases than SRES A2 (Rogelj et al. 2012).

Future temperature changes tend to be larger at higher altitudes with a spatial correlation coefficient between mean temperature changes and topography of 0.82. This clear dependence of near-surface temperature changes on elevation (see Fig. S6 in the Supplementary Material) is likely related with the effect of the SAF that enhances climate sensitivity in climate change simulations (Sellers 1969; Robock 1983; Qu and Hall 2007) due to changes in the albedo of the snow-affected regions as near-surface temperature increases. As shown in Fig. S6 in Supplementary Material, differences in maximum temperature changes between low and high elevations can attain nearly 1 °C thus explaining more than one third of the total change. Using an ensemble of RCM simulations, Steger et al. (2013) also found larger warming at higher elevations over the Swiss Alps with differences of the order of 1 °C between low and high elevation areas during winter months. Their results show that the elevation dependence of temperature changes varies across different RCMs. Using an ensemble of RCM simulations, Winter et al. (2017) found a large range of SAF sensitivities and showed that while some RCMs provide a good estimation of the observed SAF, others overestimate its value. Further work is needed to assess the ability of the NARCliM ensemble to simulate the SAF effect over the Australian alpine region.

The SAF effect is likely at the source of the differential warming at different elevations but might also explain the larger warming rates of maximum compared to minimum temperatures as the SAF effect is larger during the day (it involves short-wave radiation through changes in the albedo) thus affecting more importantly the maximum than the minimum temperatures. In agreement with these results, Grose et al. (2015a) also showed that future changes in maximum temperatures are larger than those in minimum temperatures although only when considering results from their dynamical downscaling approach (see CCAM results in Fig. 4.2.7). Again, this suggests that the failure of coarse-resolution GCMs to represent the complex topography (and high elevations) of the Australian Alps prevents CMIP5 models from simulating the SAF effect including the different warming rates in maximum and minimum temperatures.

In general, far-future temperature changes as obtained using the BC data (see Figs. S7a,c in the Supplementary Material) differ little with those obtained using the raw data. BC far future changes tend to show a somewhat stronger warming (see Table 4) and a slightly different spatial pattern with a weaker dependence on elevation compared to the raw data (spatial correlation with elevation is 0.68 in the BC and 0.82 in the raw data). Far-future changes in monthly mean temperatures (Fig. 9c, d) show that while all members exhibit significant warming, the magnitude of the changes can differ substantially across them. Warming rates are largely controlled by the choice of the driving GCM with largest rates for simulations performed using MIROC3.2 and smallest rates for simulations using either CSIRO-MK3.0 or ECHAM5, depending on the month. An interesting feature shown by most members is an increase in warming rates towards the end of the snow season, particularly when considering maximum temperature changes (not shown). Such a response is consistent with the snow-albedo feedback effect that tends to be more important at the end of the snow season (Robock 1983; Qu and Hall 2007). Again, this response was also observed by Grose et al. (2015a) particularly when considering results derived using the high-resolution CCAM model (see their Fig. 4.2.7).

Table 4 Averaged future changes in near surface mean temperature, total precipitation (*PR*) and Ruddell-derived snow (*RSR*) and rain (*RRR*) rates for near and far future periods

Data	Period	ΔT_{mean} (°C)	Δ *PR* (%)	Δ *RSR* (%)	Δ *RRR* (%)
Raw	2020–2039	0.54	−2	−8	6
	2060–2079	1.9	−7	−35	33
BC	2020–2039	0.57	−2	−7	11
	2060–2079	2.02	−7	−29	55

Results for the raw and BC datasets are shown. Precipitation changes (in %) are presented relative to present climate (1990–2009) values. Areal-mean values are calculated using grid points that have regular snow cover in all three periods. Results are only shown for the ensemble mean. Grid points with regular snow cover verify that the seasonal SCD is larger than 1 day in at least 75% of the period

Figure 9b shows that total precipitation rates are projected to decrease over the Australian alpine region although these projections are much less robust than in the temperature case. Far future projected changes suggest an areal-mean decrease of about 7% compared with present-day precipitation rates for both the raw and BC datasets (see Table 4). As shown in Fig. 9d, regardless of the dataset, the largest and more robust precipitation decreases occur at the end of the snow season (in September and October) with all members of the ensemble agreeing on the drying. The general decrease in winter and particularly in spring precipitation as shown by the NARCliM ensemble is in agreement with results from CMIP5 GCM models and downscaled projections (CSIRO and Bureau of Meteorology 2015). Again, a direct comparison is precluded due to differences in both the region and period of analysis but results from CMIP5 GCM models and CCAM in CSIRO and Bureau of Meteorology (2015) suggest somewhat smaller reductions on spring precipitation (about 15%) than in NARCliM (about 30%). As discussed by Grose et al. (2015b), this springtime drying appears to be related with a substantial strengthening of the subtropical ridge.

Despite the general decrease in total precipitation, rain rates as derived using the Ruddell equation (top panels in Fig. S8 in Supplementary Material) are projected to increase due to a much larger proportion of precipitation falling as rain as a consequence of the temperature increases. Rain rate increases vary across the Australian alpine region with an overall increase of about 33% (55%) and largest values of 59% (81%) over high elevation regions for the raw (BC) data. Projected changes in rain rates are much more robust than those in total precipitation as a consequence of their dependence on temperature projections. Consistent with the above results, snow rates (bottom panels in Fig. S8 in Supplementary Material) show very large decreases that are statistically significant over the whole Australian alpine region. Snow rate decreases averaged about 30% over the region although they are projected to attain 65% in some grid points, mainly over low elevations. Table 4 summarises temperature and precipitation changes for both future periods and for the raw and the BC datasets. Near future changes are roughly four times smaller than far future changes with mean temperature changes of 0.5 °C and precipitation changes of − 2.5% in the raw data.

Consistent with changes in temperature and snow rates, significant changes arise in the characteristics of the snowpack in future projections. In order to illustrate these changes, Fig. 10 shows daily mean SC fractions for present, near future and far future periods. Results are shown for three different grid points and for both the raw (left panels) and BC (right panels) datasets. Differences between the raw and BC datasets for a given grid point show that although the correction usually leads to a decrease of the snowpack, in some grid points an increase can be observed. For a grid point situated in the western flank of the mountains (Fig. 10a, b) that shows a large negative temperature bias and a large positive precipitation bias in the past climate, the correction results in a virtual disappearance of the snow cover. On the other hand, for grid points located at the peak and towards the eastern flank of the mountains (Fig. 10c–f), both showing a positive temperature bias, the correction leads to an increase in the snow fractions. As expected, regardless of the grid point considered and the dataset, the snow season will start later and will finish earlier in the future compared to the present climate thus leading to lower mean snow cover fractions in the future. Snow cover fraction decreases are much larger in the far future than in the near future.

Figure 11 shows far-future changes in the snow cover characteristics for the raw (left panels) and the BC (right panels) datasets. The projected changes show significant decreases everywhere and the spatial distribution (Fig. 11a, b) shows that decreases are correlated with elevation with larger decreases occurring over higher elevations (spatial correlation of − 0.75 and − 0.55 for the raw and the BC data respectively). The elevation dependence seems to arise from the combined effect of temperature changes (larger in higher altitudes) and present-day snow cover values (also larger in higher elevations). In relative terms (Fig. 11c, d), the NARCliM raw ensemble mean suggests quite uniform changes while the BC data shows more heterogeneous results with higher changes over lower elevations.

The reduction in the total snow cover can also be quantified by counting the number of grid points with regular snow cover in all three periods. According to the raw data, the number of grid points decreases from a value of 270 in the present to 228 (− 15%) to 114 (− 57%) in the near and far future periods respectively. The number of snow-covered grid points in the BC data changes from 67 to 53 (− 21%) and 24 (− 64%) for the same periods. These results suggest similar relative changes with a somewhat greater reduction in the BC data. Another way to look at future changes is by evaluating areal mean values for those grid points that show regular snow cover in present and future periods (i.e., looking at common grid points across the three periods). Table 5 shows that the mean snow cover fraction in the raw data is reduced by 15 and 54% compared to present day climate for near and far future respectively. For the same periods, the BC data shows nearly the same reductions (15 and 52% respectively). Table 5 also presents areal-mean values for the start, end and mean duration of the snow season. In both the raw and BC datasets, the duration of the snow season decreases by about 10% by 2020–2039 (12 days compared with present climate) and about 40% by 2060–2079 (45 days). The shortening of the snow season occurs due to a later start of ~ 21 days and an earlier melt of 24 days for the raw and BC data respectively. That is, our results show a weak asymmetry in the sortening of the snow season with stronger shortening in springtime. A similar asymmetry was found by Steger et al. (2013) in their study over the Swiss Alps although their found greater differences between the shortening at start and the end.

In general, future changes as a fraction of the present values are remarkably similar in both datasets. The only significant difference is a somewhat greater reduction in the number of regularly snow-covered grid points in the BC dataset. The BC data show larger rates of snow cover reduction per degree of warming with an areal-mean value of − 0.083 °C^{-1} compared with a value of − 0.056 °C^{-1} for the raw data. These differences might be related with the initial distribution of snow cover mean values although further work is needed to better understand some of the differences between the raw and BC datasets.

The snowpack reductions found in this study are of similar magnitude to those found in other studies. For example, Steger et al. (2013) found that snow water equivalent reductions were strongly dependent on the altitude (in relative terms, higher for lower elevations) with reductions

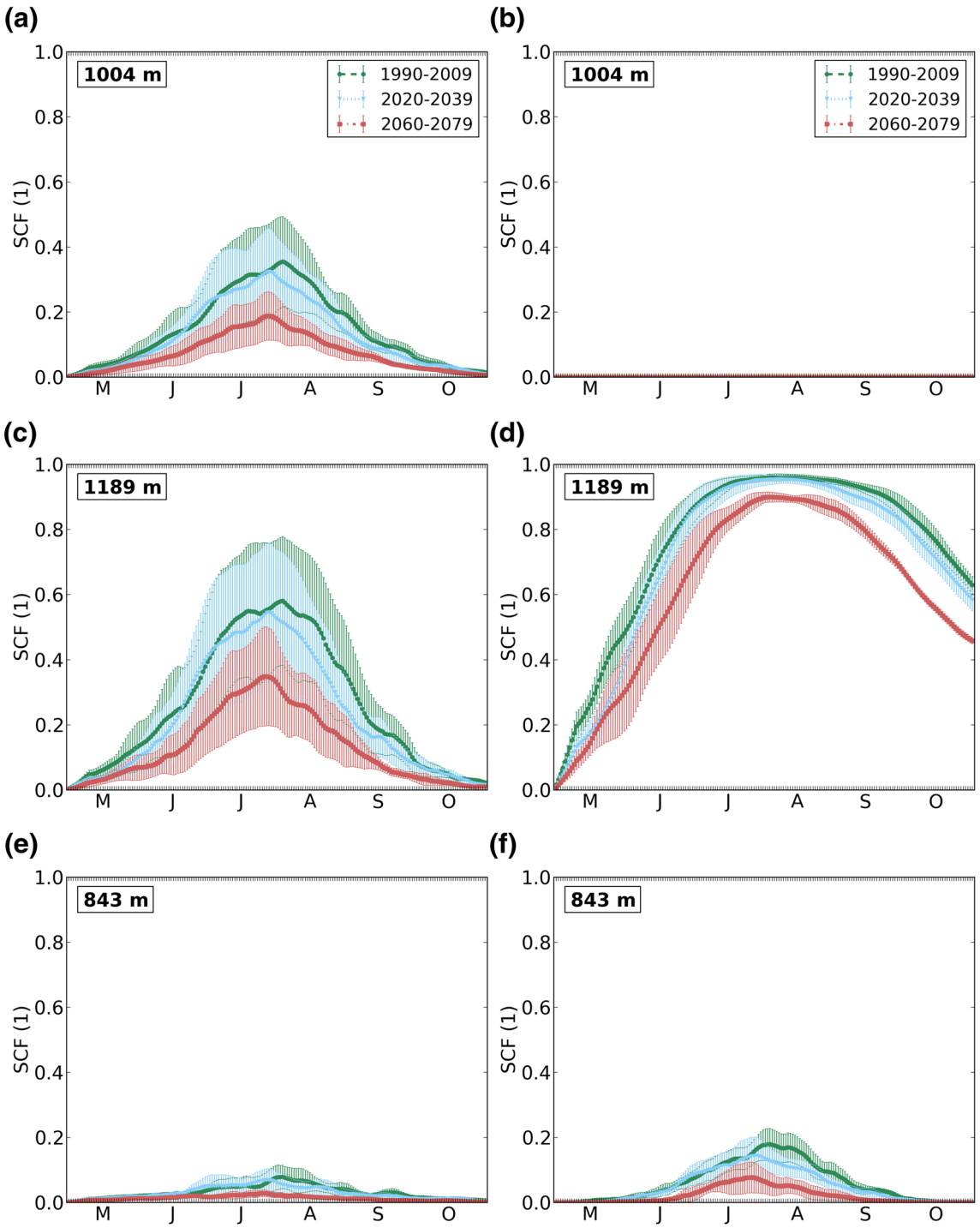

Fig. 10 Daily mean snow cover fraction for present, near future and far future periods for the raw (left panels) and the BC (right panels) NARCliM data. Top, middle and bottom panels show results for three distinct grid points located at the same latitude (36.5°S) and longitudes of 147.8, 148.3 and 148.5°E respectively. The ensemble mean is shown with the thick line and error bars show one standard deviation of the members distribution. The elevation of each grid box is shown in the top left corner

of about 70% for elevations below 1000 m. For the snow water equivalent, our estimations suggest a reduction of 69 and 61% for the period 2060–2079 (see Table 5) although these results are not directly comparable due to

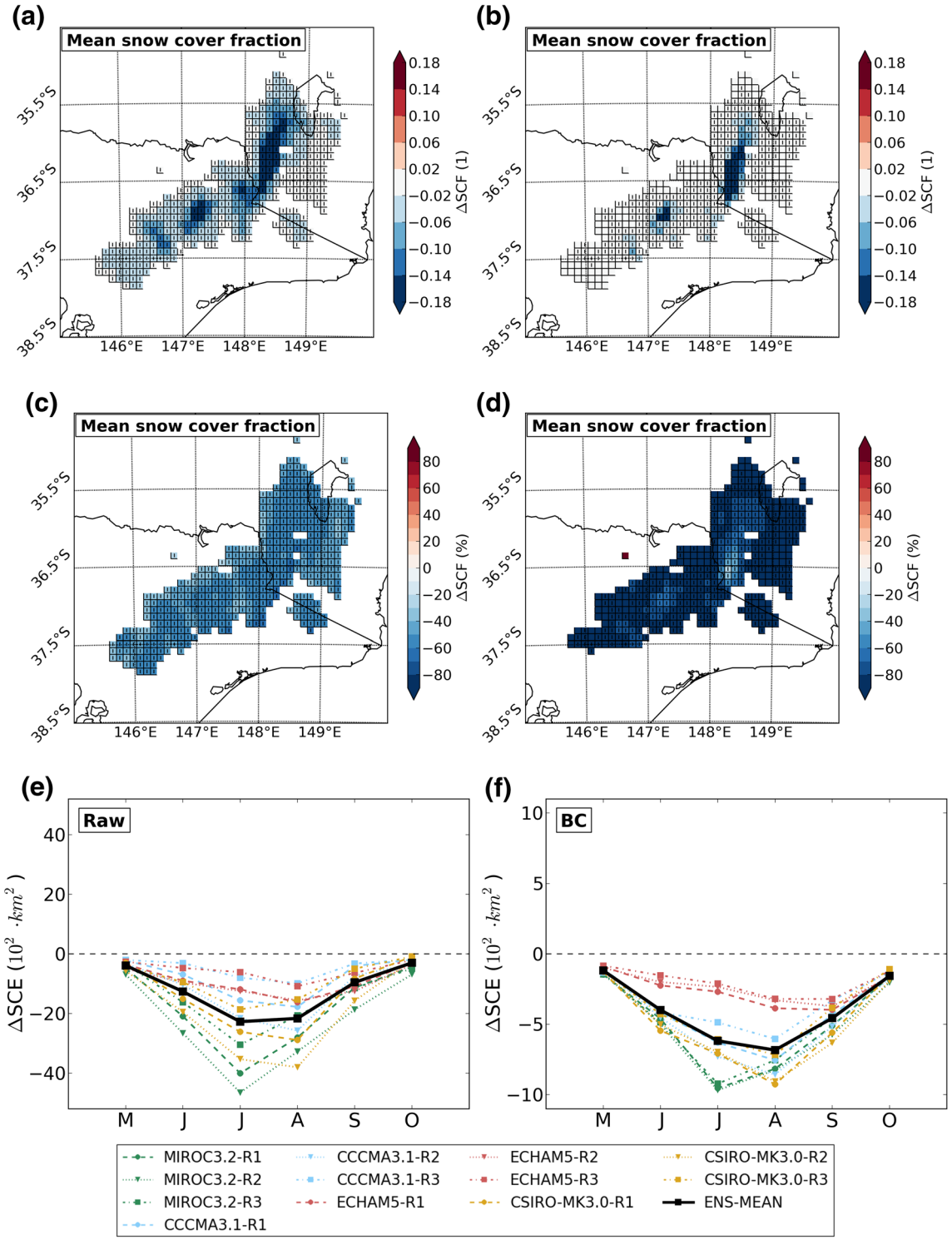

Fig. 11 Far-future (2060–2079) projected changes of mean snow cover fraction for the raw (left panels) and the BC (right panels) data. Top panels show absolute changes, middle panels relative changes and bottom panels monthly mean changes. All changes are calculated compared to the present-day (1990–2009) climatology. Top and middle panels show results for the ensemble mean and the stippling provides information about the significance and agreement across models. In bottom panels, areal-mean values are calculated using grid points that have regular snow cover in all three periods

Table 5 Areal mean values for the raw and BC data and for different periods

Data	Period	SCF (1)	SCOD (DOY)	SCMD (DOY)	SCD (days)	SWE (mm)	SD (cm)
	1990–2009	0.2	157	266	108	12.2	4.2
Raw	2020–2039	0.17 (−15)	164	260	96 (−11)	9.6 (−21)	3.3 (−20)
	2060–2079	0.09 (−54)	179	242	63 (−41)	3.7 (−69)	1.3 (−69)
	1990–2009	0.32	154	272	117	55.9	13.6
BC	2020–2039	0.27 (−15)	161	267	105 (−10)	46.0 (−17)	11.3 (−16)
	2060–2079	0.15 (−52)	175	248	72 (−38)	21.4 (−61)	5.5 (-59)

Several seasonal descriptors are shown including SC fraction, SC onset day, SC melt day, SC duration, snow water equivalent and snow depth. Areal-mean values are calculated using grid points that have regular snow cover in all three periods. Results are shown only for the ensemble mean. Relative changes (in %) compared to present climate (1990–2009) are included in parentheses. Grid points with regular snow cover verify that the seasonal SCD is larger than 1 day in at least 75% of the period

differences in the scenario (distinct future warming) and analysis period (2071–2099).

8 Uncertainties in future projections

Far-future changes in monthly mean values (Fig. 11e, f) show that the largest changes in snowpack characteristics occur on the core winter months in both NARCliM datasets. Figure 11e, f also show that the uncertainty of the projections is quite large and generally dominated by the choice of the GCM, particularly when considering the BC data (left panels). Particularly for the snow cover extent, the BC data show smaller uncertainties compared to the raw data. However, a more detailed analysis of future uncertainties suggests that the reduction of the uncertainties in the BC data depends on the specific variable being considered. Table 6 presents an estimation of future changes uncertainties for both datasets and both future periods based on the inter-member standard deviation. Results show that for some variables uncertainties appear to be larger for the BC dataset.

In order to gain more insight on the sources of the uncertainties, we have decomposed the full variance according to the choice of the GCM, the RCM and the sampling uncertainty. The variance decomposition method as applied here follows directly from Déqué et al. (2007) and Di Luca et al. (2014). The sampling uncertainty was estimated using a Monte Carlo approach as described in Section 1 of the Supplementary Material. The climate change signal of a given variable V can then be expressed as $\Delta V_{GRI} \in \Re^{4\times3\times100}$ where index G denotes the choice of the GCM ($\in [0,3]$), R the choice of the RCM ($\in [0,2]$) and I the choice of the random sample ($\in [0,99]$) calculated using the Monte Carlo approach.

Figure 12 presents results for (a) near and (b) far future changes. Single terms (i.e., G, R, and I) represent the contribution to the total variance coming from that index when averaging over the remaining indices. That is, the term R will be different from zero if the mean change is different in the three RCM configurations. Second order terms of the form GR, GI, RI represent the contribution of the interaction between two given sources (e.g. RCM and GCM) to the total uncertainty. For example, they might reflect whether some RCM uncertainties depend on the specific driving GCM (i.e. GCM-dependent RCM differences). Fig. 12 shows that the influence of the sampling term (i.e., of the internal variability) is much greater for near than far future projections due to the relatively smaller effect of greenhouse gases by 2020–2039. By 2060–2079, however, intermodel differences (uncertainty due to the choice of RCM and GCM) explain about 90% of the total variance for most variables showing that the sampling uncertainty becomes small on the long term. Regardless of the variable considered, the choice of the GCM dominates the full uncertainty with values higher than 60% for some variables. The contribution to the full uncertainty from the choice of the RCM is however not

Table 6 Climate change uncertainties for the raw and bias corrected datasets and near and far future periods

Period	Data	T_{mean} (°C)	PR (mm)	RSR (mm)	RRR (mm)	SWE (mm)	SD (cm)	SCF
2020–2039	Raw	0.16	0.29	0.21	0.22	1.13	0.35	0.01
	BC	0.2	0.22	0.17	0.16	1.89	0.45	0.01
2060–2079	Raw	0.24	0.47	0.32	0.31	1.81	0.57	0.019
	BC	0.32	0.35	0.23	0.31	2.09	0.51	0.011

Uncertainties are estimated by calculating the total standard deviation of the a climate change distribution that includes the 12 member NARCliM ensemble. Several variables are included: snow depth (SD), snow water equivalent (SWE), snow cover fraction (SCF), mean temperature (T_{mean}), total precipitation rate (PR), Ruddell rain rate (RRR) and Ruddell snow rate (RSR)

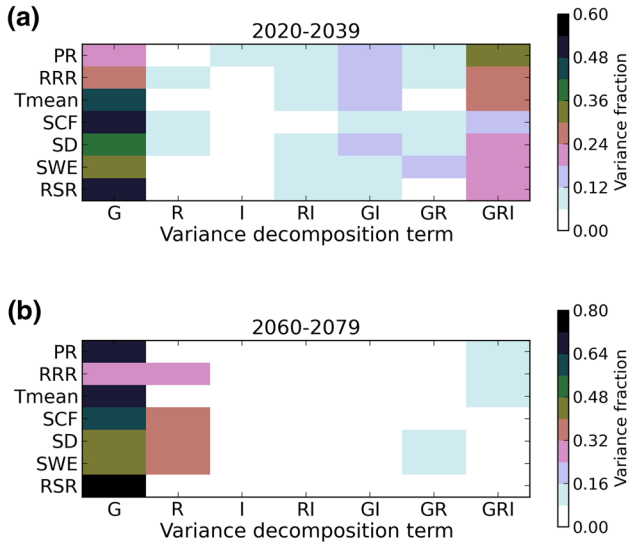

Fig. 12 Fraction of the total uncertainty explained by the various decomposition terms for **a** near (2020–2039) and **b** far-future (2060–2079) projected changes based on the raw data. In the variance decomposition terms, *G* represents the boundary conditions (GCMs), *R* the RCM and *I* the sampling uncertainty. Details about the decomposition method are given in Di Luca et al. (2014). Results are shown for snow depth (SD), Ruddell snow rate (RSR), snow water equivalent (SWE), snow cover fraction (SCF), mean temperature (T_{mean}), Ruddell rain rate (RRR) and total precipitation rate (PR). Only results for the raw data are shown

negligible with values close to 30% depending on the specific variable being considered.

9 Discussion and conclusions

Using a range of observations, a number of studies have shown a general warming and a decrease of the snowpack over the Australian alpine region suggesting that climate changes related with the increase of greenhouse gases might be already occurring. Given the high vulnerability of the Australian alpine snow fields to changes in the climate, there is a clear need to assess and understand possible future climate changes and provide plausible scenarios to be used by the impact, adaptation and mitigation communities.

In this article, we have presented an analysis of the Australian Alps snowpack characteristics and other related variables in observations (in situ gridded and satellite data) and in a high-resolution regional climate model (RCM) ensemble. The study included the evaluation of the ability of the ensemble to simulate the observed snowpack characteristics over the period 2000–2009, the development of a bias correction technique and the estimation of future projections based on two future periods (2020–2039 and 2060–2079). The RCM ensemble used here was performed within the NSW/ACT Regional Climate Modelling (NARCliM) project and consists of a total of 12 simulations, all at 10-km grid spacing, carried out using four GCMs from CMIP3 (all following the A2 scenario) and three different WRF configurations.

The evaluation of the NARCliM ensemble showed that all simulations have a negative temperature bias, largely related with an underestimation of maximum temperatures, and that they produce too much precipitation mostly in the western flank of the Australian Alps. We applied a multiple linear regression analysis and found that about 55% of the seasonal-mean snow cover errors can be explained using minimum, maximum and total precipitation errors as predictors with maximum temperature errors playing the leading role.

We then apply the quantile mapping method using theoretical functions (Piani et al. 2010) to correct simulated temperature and precipitation time series with the aid of the AWAP gridded observations. Prior to the application of the correction for precipitation fields, the total precipitation is decomposed in rain and snow based on an empirical relationship and the corrected daily minimum temperature. The correction is then performed independently for the rain and snowfall terms. The corrected time series are then used to force a temperature based snow melt/accumulation model to produce new, bias corrected, estimations of snow depth, snow water equivalent and snow cover.

The present climate bias corrected (BC) snowpack shows important differences compared with the raw data and, although some positive biases remain, the BC data show large improvements regarding the simulation of total amounts, seasonality and spatial distribution of the snow cover compared with the MODIS products. In addition to the improvements in the snow cover representation, the BC ensemble indicates a general reduction of the present climate uncertainty associated with individual members compared with the raw data.

NARCliM simulations project robust future increases of near surface temperatures with a clear influence of the snow-albedo feedback effect that enhances the warming at higher elevations. While generally not significant, future precipitation changes suggest a decrease of the total precipitation by 2070 mostly due to a drying in springtime. Simulations project significant decreases in snow rates and increases in rain rates due to changes in the occurrence of solid and liquid precipitation phases related to the temperature changes. Rain increases are observed in spite of a the general small decrease in total precipitation.

As a consequence of the steady decreases in snowfall and increases in temperature, projections show a substantial reduction of the snowpack over the Australian Alps. A summary of the NARCliM ensemble mean climatology of snow cover extent for present (1990–2009), near-future (2020–2039) and far-future (2060–2079) is given in top panels in Fig. 13. In both datasets, snow cover extent decreases

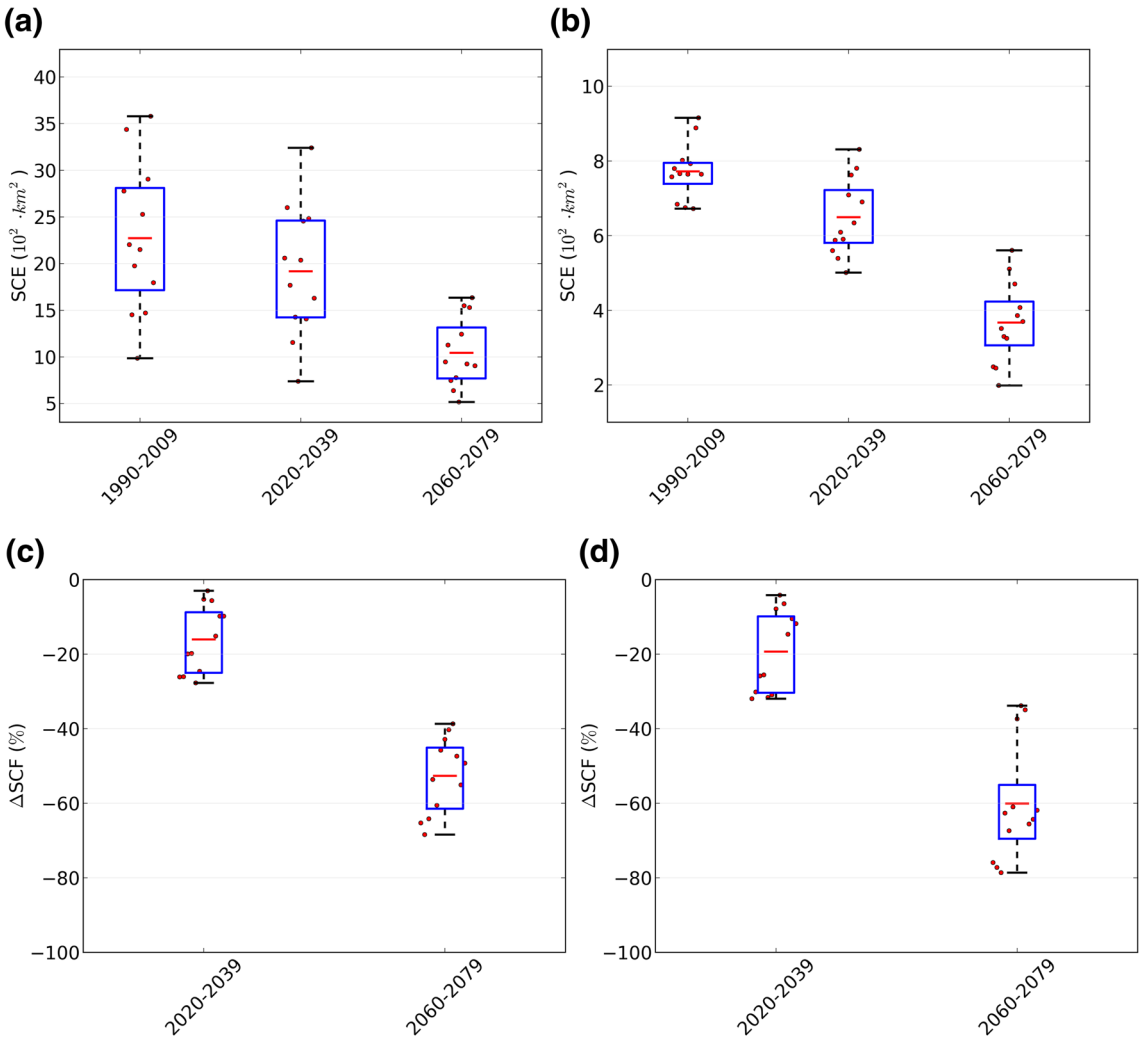

Fig. 13 Snow cover mean extent (top panels) and changes relative to present values (bottom panels) for present, near future and far future climates. Left and right panels show results for the NARCliM raw and BC datasets respectively. Areal-mean values are calculated using grid points that have regular snow cover in all three periods. The NARCliM ensemble mean (red line), inter-quartile range (blue box) and total range (whisker) are shown for each period. Red circles represent values from individual members

by about 15 and 60% by 2030 and 2070 respectively. It is interesting to note that while the BC data introduces large differences in the simulation of the present climate snow cover (e.g., SCE is about three times smaller in the BC than in the raw data), in relative terms future changes appear to be similar in both datasets. The BC data only suggest slightly larger relative changes in the snowpack, presumably explained by a somewhat different spatial distribution of the temperature changes. The strong agreement between changes obtained in both datasets suggests that the BC data can be safely used in order to provide more coherent present and future scenarios for adaptation strategies.

Future projections of snowpack characteristics show large uncertainties due to both the choice of the lateral boundary conditions (i.e., the GCM) and the choice of the RCM version although dominated by the former. Near-future uncertainties show a non-negligable influence of the internal variability (i.e., sampling) term, here estimated using a Monte Carlo approach. Although the BC data suggests a small reduction of the uncertainty compared with the raw data when looking at the snow cover extent, the consideration of other variables (e.g. snow water equivalent) shows that undertainties in the BC data might be larger than in the raw data.

It is important to mention a number of limitations of this study. First, the evaluation and correction of NARCliM simulations was performed using observations that are characterised by important uncertainties and even some systematic errors. Specifically, as mentioned in the Data Section, AWAP systematically underestimates total precipitation over the western slopes during winter months (Chubb et al. 2015, 2016). Also, the uncertainty associated with the two MODIS

derived products used in this study is very large and it is unclear which dataset gives better results.

Second, the RCM ensemble used here is limited in some regards. Future simulations have been performed using a single scenario of emissions (SRES A2, Nakićenović et al. 2000). It is expected, however, that a simple temperature scaling could account for differences with other scenarios. The RCM ensemble is also relatively small (12 members) although RCMs and GCMs were selected based on their independence thus allowing to sample more effectively future model uncertainty.

Third, the future snowpack using corrected input fields was estimated based on a simple temperature index melt snow model. Although temperature index models have shown good performance and continue to be widely used, it is expected that a more physically based energy balance model can provide better snowpack estimations, particularly when looking at high spatiotemporal resolution results (Hock 2003). Ongoing and future work will try to address some of this limitations.

Acknowledgements Support for this work was provided by the New South Wales (NSW) Office of Environment and Heritage to build on the NSW/ACT Regional Climate Modelling (NARCliM) Project. This work was made possible through the Merit Allocation Scheme award from the NCI (National Computational Infrastructure) National Facility at the Australian National University. The authors would like to thank Kathryn J. Bormann and Jeffery A. Thompson for providing the MODIS derived satellite datasets and the scientists involved in generating AWAP observational datasets that are used in this study. The authors also acknowledge the administration of Climate Change Research Centre at the University of New South Wales for the logistical support, the modelling groups, the Program for Climate Model Diagnosis and Intercomparison (PCMDI) and the WCRP's Working Group on Coupled Modelling (WGCM) for their roles in making available the World Climate Research Programme (WCRP) CMIP3 multimodel data set. Support of this data set is provided by the Office of Science, U.S. Department of Energy. We thank the scientists at NCAR Mesoscale and Microscale Meteorology Division for maintaining the Weather Research and Forecasting Model.

References

Argüeso D, Evans JP, Fita L (2013) Precipitation bias correction of very high resolution regional climate models. Hydrol Earth Syst Sci 17:4379–4388. doi:10.5194/hess-17-4379-2013

Argüeso D, Evans JP, Fita L (2013) Precipitation bias correction of very high resolution regional climate models. Hydrol Earth Syst Sci 17(11):4379–4388. doi:10.5194/hess-17-4379-2013

Auer AH Jr (1974) The rain versus snow threshold temperatures. Weatherwise 27(2):67–67. doi:10.1080/00431672.1974.9931684

Bellprat O, Kotlarski S, Lüthi D, Schär C (2013) Physical constraints for temperature biases in climate models. Geophys Res Lett 40(15):4042–4047. doi:10.1002/grl.50737

Bhend J, Bathols J, Hennessy K (2012) Climate change impacts on snow in Victoria, vol 42. CSIRO report for the Victorian Department of Sustainability and Environment, Aspendale

Bishop CH, Abramowitz G (2013) Climate model dependence and the replicate Earth paradigm. Clim Dyn 41(3–4):885–900. doi:10.1007/s00382-012-1610-y

Bormann K, McCabe M, Evans JP (2012a) Satellite based observations for seasonal snow cover detection and characterisation in Australia. Remote Sens Environ 123:57–71. doi:10.1016/j.rse.2012.03.003

Bormann K, McCabe M, Evans JP (2012b) Spatial and temporal variability in seasonal snow density. J Hydrol 484:63–73. doi:10.1016/j.jhydrol.2013.01.032

Bormann K, Evans JP, McCabe M (2014) Constraining snowmelt in a temperature-index model using simulated snow densities. J Hydrol 517:652–667. doi:10.1016/j.jhydrol.2014.05.073

Brereton R, Bennett S, Mansergh I (1995) Enhanced greenhouse climate change and its potential effect on selected fauna of south-eastern australia: a trend analysis. Biol Conserv 72(3):339–354. doi:10.1016/0006-3207(94)00016-J

Brown RD, Mote PW (2009) The response of Northern Hemisphere Snow cover to a changing climate. J Clim 22(8):2124–2145. doi:10.1175/2008JCLI2665.1

Chen F, Dudhia J (2001) Coupling an advanced land surfacehydrology model with the Penn State NCAR MM5 modeling system. Part I: model implementation and sensitivity. Mon Weather Rev 129(4):569–585

Chubb T, Manton MJ, Siems ST, Peace AD, Bilish SP (2015) Estimation of wind-induced losses from a precipitation gauge network in the australian snowy mountains. J Hydrometeorol 16(6):2619–2638. doi:10.1175/JHM-D-14-0216.1

Chubb T, Manton M, Siems S, Peace A (2016) Evaluation of the awap daily precipitation spatial analysis with an independent gauge network in the snowy mountains. J South Hemisphere Earth Syst Sci 66:55–67

Chubb TH, Siems ST, Manton MJ (2011) On the Decline of wintertime precipitation in the snowy mountains of Southeastern Australia. J Hydrometeorol 12(6):1483–1497. doi:10.1175/JHM-D-10-05021.1

Chylek P, McCabe M, Dubey MK, Dozier J (2007) Remote sensing of Greenland ice sheet using multispectral near-infrared and visible radiances. J Geophys Res. doi:10.1029/2007JD008742

Crane RG, Anderson MR (1984) Satellite discrimination of snow/cloud surfaces. Int J Remote Sens 5(1):213–223. doi:10.1080/01431168408948799

CSIRO, Bureau of Meteorology, (2015) Climate change in Australia information for Australias natural resource management regions: technical report. Tech. rep, CSIRO and Bureau of Meteorology, Australia

Da Ronco P, De Michele C, Montesarchio M, Mercogliano P (2016) Comparing COSMO-CLM simulations and MODIS data of snow cover extent and distribution over Italian Alps. Clim Dyn. doi:10.1007/s00382-016-3054-2.

Dai A (2008) Temperature and pressure dependence of the rain-snow phase transition over land and ocean. Geophys Res Lett. doi:10.1029/2008GL033295.

Davis C (2013) Towards the development of long-term winter records for the snowy mountains. Aust Meteorol Oceanogr J 63(2):303–314

Déqué M, Rowell DP, Lüthi D, Giorgi F, Christensen JH, Rockel B, Jacob D, Kjellström E, Castro M, Hurk B (2007) An intercomparison of regional climate simulations for Europe: assessing uncertainties in model projections. Clim Change 81(S1):53–70. doi:10.1007/s10584-006-9228-x

Di Luca A, de Elía R, Laprise R (2013) Potential for added value in temperature simulated by high-resolution nested RCMs in present climate and in the climate change signal. Clim Dyn 40(1–2):443–464. doi:10.1007/s00382-012-1415-z

Di Luca A, Flaounas E, Drobinski P, Brossier C (2014) The atmospheric component of the Mediterranean Sea water budget in a WRF multi-physics ensemble and observations. Clim Dyn. doi:10.1007/s00382-014-2058-z

Di Luca A, Argüeso D, Evans JP, de Elía R, Laprise R (2016) Quantifying the overall added value of dynamical downscaling and the contribution from different spatial scales. J Geophys Res Atmos 121(4):1575–1590. doi:10.1002/2015JD024009

Ek MB (2003) Implementation of Noah land surface model advances in the National Centers for Environmental Prediction operational mesoscale Eta model. J Geophys Res. doi:10.1029/2002JD003296

Evans JP, Ji F (2012a) Choosing GCMs. NARCliM Technical Note 1, NARCliM Consortium, Sydney, Australia

Evans JP, Ji F (2012b) Choosing the RCMs to perform the downscaling. NARCliM Technical Note 2, NARCliM Consortium, Sydney, Australia

Evans JP, Ji F, Lee C, Smith P, Argüeso D, Fita L (2014) Design of a regional climate modelling projection ensemble experiment—NARCliM. Geosci Model Dev 7(2):621–629. doi:10.5194/gmd-7-621-2014

Evans JP, Bormann K, Katzfey J, Dean S, Arritt R (2016) Regional climate model projections of the South Pacific Convergence Zone. Clim Dyn 47(3–4):817–829. doi:10.1007/s00382-015-2873-x

Feser F, Rockel B, von Storch H, Winterfeldt J, Zahn M (2011) Regional climate models add value to global model data: a review and selected examples. Bull Am Meteorol Soc 92(9):1181–1192

Fiddes SL, Pezza AB, Barras V (2015) A new perspective on Australian snow. Atmos Sci Lett 16(3):246–252. doi:10.1002/asl2.549

Frei P, Kotlarski S, Liniger MA, Schär C (2017) Snowfall in the Alps: evaluation and projections based on the EURO-CORDEX regional climate models. Cryosphere Discussions. doi:10.5194/tc-2017-7

Giorgi F, Hurrell JW, Marinucci MR, Beniston M (1997) Elevation dependency of the surface climate change signal: a model study. J Clim 10(2):288–296

Giorgi F, Torma C, Coppola E, Ban N, Schär C, Somot S (2016) Enhanced summer convective rainfall at Alpine high elevations in response to climate warming. Nature Geosci advance online publication

Grose M, Abbs D, Bhend J, Chiew F, Church J, Ekström M, Kirono D, Lenton A, Lucas C, McInnes K, Moise A, Monselesan D, Mpelasoka F, Webb L, Whetton P (2015a) Central Slopes Clust Rep. Climate change in Australia projections for australias natural resource management regions, Cluster reports, CSIRO and Bureau of Meteorology, Australia

Grose M, Timbal B, Wilson L, Bathols J, Kent D (2015b) The subtropical ridge in CMIP5 models, and implications for projections of rainfall in southeast Australia. Aust Meteorol Oceanogr J 65:90–106

Gudmundsson L, Bremnes JB, Haugen JE, Engen-Skaugen T (2012) Technical note: downscaling RCM precipitation to the station scale using statistical transformations—a comparison of methods. Hydrol Earth Syst Sci 16(9):3383–3390. doi:10.5194/hess-16-3383-2012

Hall DK, Riggs GA, Salomonson VV, DiGirolamo NE, Bayr KJ (2002) MODIS snow-cover products. Remote Sens Environ 83(1):181–194

Hennessy K, Whetton P, Walsh K, Smith I, Bathols J, Hutchinson M, Sharples J (2008) Climate change effects on snow conditions in mainland Australia and adaptation at SKI resorts through snowmaking. Clim Res 35(3):255–270

Hock R (2003) Temperature index melt modelling in mountain areas. J Hydrol 282(1–4):104–115. doi:10.1016/S0022-1694(03)00257-9

Hughes L (2003) Climate change and australia: trends, projections and impacts. Austral Ecol 28(4):423–443. doi:10.1046/j.1442-9993.2003.01300.x

Ivanov M, Kotlarski S (2016) Assessing distribution-based climate model bias correction methods over an alpine domain: added value and limitations. Int J Climatol. doi:10.1002/joc.4870

Ji F, Evans JP, Teng J, Scorgie Y, Argüeso D, Di Luca A (2016) Evaluation of long-term precipitation and temperature Weather Research and Forecasting simulations for southeast Australia. Clim Res 67(2):99–115. doi:10.3354/cr01366

Jones DA, Wang W, Fawcett R (2009) High-quality spatial climate data-sets for Australia. Aust Meteorol Oceanogr J 58(4):233–248

Kienzle SW (2008) A new temperature based method to separate rain and snow. Hydrol Process 22(26):5067–5085. doi:10.1002/hyp.7131

King AD, Alexander LV, Donat MG (2013) The efficacy of using gridded data to examine extreme rainfall characteristics: a case study for Australia. Int J Climatol 33(10):2376–2387. doi:10.1002/joc.3588

Kotlarski S, Bosshard T, Lüthi D, Pall P, Schär C (2012) Elevation gradients of European climate change in the regional climate model COSMO-CLM. Clim Change 112(2):189–215. doi:10.1007/s10584-011-0195-5

Kotlarski S, Keuler K, Christensen OB, Colette A, Dqu M, Gobiet A, Goergen K, Jacob D, Lüthi D, van Meijgaard E, Nikulin G, Schär C, Teichmann C, Vautard R, Warrach-Sagi K, Wulfmeyer V (2014) Regional climate modeling on European scales: a joint standard evaluation of the EURO-CORDEX RCM ensemble. Geosci Model Dev 7(4):1297–1333. doi:10.5194/gmd-7-1297-2014

Maraun D (2012) Nonstationarities of regional climate model biases in European seasonal mean temperature and precipitation sums. Geophys Res Lett. doi:10.1029/2012GL051210

Nakićenović N, Alcamo J, Davis G, de Vries B, Fenhann J, Gaffin S, Gregory K, Grübler A, Jung TY, Kram T, Lebre La Rovere E, Michaelis L, Mori S, Morita T, Pepper W, Pitcher H, Price L, Riahi K, Roehrl A, Rogner HH, Sankovski A, Schlesinger M, Shukla P, Smith S, Swart R, van Rooijen S, Victor N, Dadi Z (2000) IPCC Special report on emissions scenarios (SRES). Cambridge University Press, UK

Nicholls N (2005) Climate variability, climate change and the Australian snow season. Aust Meteorol Mag 54(3):177–185

Olson R, Evans JP, Di Luca A, Argüeso D (2016) The NARCliM project: model agreement and significance of climate projections. Clim Res 69:209–227

Piani C, Haerter J, Coppola E (2010) Statistical bias correction for daily precipitation in regional climate models over Europe. Theor Appl Climatol 99(1–2):187–192. doi:10.1007/s00704-009-0134-9

Pickering C, Armstrong T (2003) The potential impacts of climate change on plant communities in the Kosciuszko alpine zone. Victorian Nat 120(1):15–23

Prein A, Gobiet A, Truhetz H, Keuler K, Goergen K, Teichmann C, Fox Maule C, van Meijgaard E, Déqué M, Nikulin G, Vautard R, Colette A, Kjellström E, Jacob D (2015) Precipitation in the euro-cordex 0.11° and 0.44° simulations: high resolution, high benefits? Clim Dyn. doi:10.1007/s00382-015-2589-y

Prömmel K, Geyer B (2010) Evaluation of the skill and added value of a reanalysisdriven regional simulation for Alpine temperature. Int J Climatol. doi:10.1002/joc.1916

Qu X, Hall A (2007) What controls the strength of Snow-Albedo feedback? J Clim 20(15):3971–3981. doi:10.1175/JCLI4186.1

Riggs G, Hall D, Salomonson V (2006) MODIS Snow Products User Guide to Collection 5 George A. Riggs. Tech. rep

Robock A (1983) Ice and snow feedbacks and the latitudinal and seasonal distribution of climate sensitivity. Journal of the Atmospheric Sciences 40(4):986–997. doi:10.1175/1520-0469(1983)040<0986:IASFAT>2.0.CO;2

Rogelj J, Meinshausen M, Knutti R (2012) Global warming under old and new scenarios using IPCC climate sensitivity range estimates. Nat Clim Change 2(4):248–253. doi:10.1038/nclimate1385

Ruddell A, Budd WF, Smith IN, Keage PL, Jones R (1990) The south east Australian alpine climate study: a report by the Meteorology Department, University of Melbourne for the Alpine Resorts Commission. Department of Meteorology, University of Melbourne

Schmidli J, Goodess CM, Frei C, Haylock MR, Hundecha Y, Ribalaygua J, Schmith T (2007) Statistical and dynamical downscaling of precipitation: an evaluation and comparison of scenarios for the European Alps. J Geophys Res. doi:10.1029/2005JD007026

Sellers W (1969) A global climatic model based on the energy balance of the earth-atmosphere system. Journal of Applied Meteorology 8(3):392–400. doi:10.1175/1520-0450(1969)008<0392:AGCMBO>2.0.CO;2

Skamarock WC, Klemp JB, Dudhia J, Gill DO, Barker DM, Duda MG, Huang XY, Wang W, Powers JG (2008) Description of the advanced research WRF Version 3. NCAR Technical Note. Tech. rep. NCAR, Boulder

Steger C, Kotlarski S, Jonas T, Schä C (2013) Alpine snow cover in a changing climate: a regional climate model perspective. Clim Dyn 41(3–4):735–754. doi:10.1007/s00382-012-1545-3

Thompson J (2016) A MODIS-derived snow climatology (2000–2014) for the Australian Alps. Clim Res 68(1):25–38. doi:10.3354/cr01379

Thompson J, Paull D, Lees B (2015) An improved liberal cloud-mask for addressing snow/cloud confusion with MODIS. Photogramm Eng Remote Sens 81(2):119–129. doi:10.14358/PERS.81.2.119

Thompson JA, Lees BG (2014) Applying object-based segmentation in the temporal domain to characterise snow seasonality. ISPRS J Photogramm Remote Sens 97:98–110. doi:10.1016/j.isprsjprs.2014.08.010

Timbal B, Drosdowsky W (2013) The relationship between the decline of Southeastern Australian rainfall and the strengthening of the subtropical ridge. Int J Climatol 33(4):1021–1034. doi:10.1002/joc.3492

Timbal B, Ekström M, Fiddes S, Grose M, Kirono DGC et al (2016) Climate change science and Victoria, Docklands, Vic. Bureau of Meteorology

Whetton P, Haylock M, Galloway R (1996) Climate change and snow-cover duration in the Australian Alps. Clim Change 32(4):447–479

Winter KJPM, Kotlarski S, Scherrer SC, Schr C (2017) The Alpine snow-albedo feedback in regional climate models. Clim Dyn 48(3–4):1109–1124. doi:10.1007/s00382-016-3130-7

Ye H, Cohen J, Rawlins M (2013) Discrimination of solid from liquid precipitation over Northern Eurasia using surface atmospheric conditions*. J Hydrometeorol 14(4):1345–1355